PHILOSOPHICAL TRANSACTIONS A

rsta.royalsocietypublishing.org

Review

Cite this article: Oughton S, Matthaeus WH, Wan M, Osman KT. 2015 Anisotropy in solar wind plasma turbulence. *Phil. Trans. R. Soc. A* **373**: 20140152.
http://dx.doi.org/10.1098/rsta.2014.0152

Accepted: 4 February 2015

One contribution of 11 to a theme issue 'Dissipation and heating in solar wind turbulence'.

Subject Areas:
solar system, astrophysics

Keywords:
turbulence, waves, anisotropy

Author for correspondence:
S. Oughton
e-mail: seano@waikato.ac.nz

Anisotropy in solar wind plasma turbulence

S. Oughton[1], W. H. Matthaeus[2], M. Wan[2] and K. T. Osman[3]

[1]Department of Mathematics, University of Waikato, Hamilton 3240, New Zealand
[2]Department of Physics and Astronomy, University of Delaware, DE 19716, USA
[3]Centre for Fusion, Space and Astrophysics, University of Warwick, Coventry CV4 7AL, UK

SO, 0000-0002-2814-7288

A review of spectral anisotropy and variance anisotropy for solar wind fluctuations is given, with the discussion covering inertial range and dissipation range scales. For the inertial range, theory, simulations and observations are more or less in accord, in that fluctuation energy is found to be primarily in modes with quasi-perpendicular wavevectors (relative to a suitably defined mean magnetic field), and also that most of the fluctuation energy is in the vector components transverse to the mean field. Energy transfer in the parallel direction and the energy levels in the parallel components are both relatively weak. In the dissipation range, observations indicate that variance anisotropy tends to decrease towards isotropic levels as the electron gyroradius is approached; spectral anisotropy results are mixed. Evidence for and against wave interpretations and turbulence interpretations of these features will be discussed. We also present new simulation results concerning evolution of variance anisotropy for different classes of initial conditions, each with typical background solar wind parameters.

1. Introduction

Ample evidence exists for *in situ* heating of the solar wind. In particular, observations of the proton temperature, $T_p(r)$, as a function of heliocentric radius, r, are well above the level associated with a pure adiabatic expansion of the medium (by factors of 10–100 in the outer heliosphere) [1]. Dissipation at shocks and

THE ROYAL SOCIETY PUBLISHING

reconnection zones, turbulent dissipation and various types of wave damping are all processes that may contribute to the heating. These situations typically involve fluctuations in the velocity and magnetic field over wide ranges of length and time scales, and in many of them *fluctuation anisotropies* may lead to enhanced (or curtailed) dissipation. For instance, if a dynamical process steers energy away from small parallel scales, this will obviously restrict the energy available to dissipation channels active at those scales, e.g. ion cyclotron damping. Here, we review two types of fluctuation anisotropy that are robustly observed in the solar wind: spectral anisotropy and variance anisotropy. A summary of the observational results is presented, along with discussion of candidate explanations for the origin of these anisotropies. Some roles they may play in the dissipation of solar wind fluctuations are also noted.

Our focus is primarily at magnetohydrodynamic (MHD) scales because, at length and time scales larger than those characteristic of proton gyromotion, the dynamics of solar wind fluctuations can often be usefully described using MHD models. The relative simplicity of these fluid models affords some advantages for theoretical and simulation work. Of course, the dynamics near (and below) proton gyroscales involves various *plasma* processes, so that in those ranges, it is appropriate to employ theoretical frameworks that retain more plasma and particle effects than MHD does. We will include some discussion related to these scales. Following traditional usage in the literature, we refer to frequencies above the proton gyrofrequency as the *dissipation range*, even though the (plasma) physics at these scales differs significantly from the viscous diffusion characteristic of Navier–Stokes dissipation (see appendix A).

This review is intended to complement existing reviews on solar wind anisotropy and related matters [2–6], and also other papers appearing in this theme issue [7–11]. Thus, we do not attempt a complete review of the literature. Familiarity with the basic features and properties of the solar wind is assumed here, as is a basic understanding of turbulence concepts like inertial range, dissipation range, spectra, correlation lengths and times, and energy cascades [12–14]. See appendix A for a terse summary.

The paper is structured as follows. We begin by defining spectral and variance anisotropies and discussing how these arise from distinct features of a vector field. Separate sections for each type of anisotropy follow, wherein we review relevant observational studies and discuss possible explanations. Some new results from compressible three-dimensional MHD simulations are also included. A short summary concludes the main body of the paper. Appendix A covers some primary points regarding spectra, spectral ranges and related ideas, and appendix B considers issues related to global and local mean magnetic fields.

2. Two types of anisotropy: definitions and distinctions

Let us write the velocity and magnetic fields in terms of mean values plus fluctuations about those means,

$$\boldsymbol{u}(\boldsymbol{x},t)=\boldsymbol{U}+\boldsymbol{v}(\boldsymbol{x},t),\quad \boldsymbol{U}=\langle\boldsymbol{u}\rangle \tag{2.1}$$

and

$$\boldsymbol{B}(\boldsymbol{x},t)=\boldsymbol{B}_0+\boldsymbol{b}(\boldsymbol{x},t),\quad \boldsymbol{B}_0=\langle\boldsymbol{B}\rangle, \tag{2.2}$$

where $\langle\cdots\rangle$ denotes an appropriate space ($\boldsymbol{x}$) and/or time (t) averaging operator, which might be global or local. Throughout this paper, the magnetic field is in Alfvén velocity units, i.e. the actual magnetic field (SI units) is $\sqrt{\mu\rho}\boldsymbol{B}$, where ρ is the mass density and μ is the magnetic permeability of the medium. We also make use of the Elsasser variables for the fluctuations, $\boldsymbol{z}^{\pm}(\boldsymbol{x},t)=\boldsymbol{v}\pm\boldsymbol{b}$, where these variables should not be confused with the Cartesian coordinate z. Usually, Cartesian mean-field-aligned coordinates are employed, with $\boldsymbol{B}_0\parallel\hat{\boldsymbol{z}}$. The circumflex indicates unit vectors, with that parallel to heliocentric radius being $\hat{\boldsymbol{R}}$, for example. To good approximation beyond approximately 0.1 AU, the mean solar wind speed is $\boldsymbol{U}=U_{\rm sw}\hat{\boldsymbol{R}}$. Other standard notation used is Alfvén speed $V_{\rm A}$, proton plasma beta $\beta_{\rm p}$, proton gyroradius $\rho_{\rm i}$, proton gyrofrequency $\Omega_{\rm ci}=2\pi f_{\rm ci}$ and proton skin depth $d_{\rm i}\equiv V_{\rm A}/\Omega_{\rm ci}$. It will sometimes be important to note that the mean field employed is a local one, and we then write $\boldsymbol{B}_0^{\rm loc}$ in place of $\boldsymbol{B}_0$ (cf. appendix B).

If the Cartesian components of the fluctuating field have unequal energies, then the field is said to exhibit *variance* (also known as component) anisotropy. For $\boldsymbol{v}$, this would mean departures from $\langle v_x^2\rangle = \langle v_y^2\rangle = \langle v_z^2\rangle$. In the solar wind, one typically has $\langle v_x^2\rangle \approx \langle v_y^2\rangle \gg \langle v_z^2\rangle$, if the averaging is over many correlation lengths, $L_{\rm cor}$, where $L_{\rm cor} \sim 10^6$ km at 1 AU [15–17].

However, considerable care is needed when interpreting observed variance anisotropy: even for a perfectly isotropic distribution of energy, calculated variances will be anisotropic(!) if, in effect, one only has access to reduced spectra (or, equivalently, to one-dimensional correlation functions). A reminder of Batchelor's [18, p. 50] original incompressible hydrodynamics demonstration is enlightening. Suppose the energy distribution is isotropic, so that its spectral tensor is $S_{ij}(\boldsymbol{k}) = (1/2)(\delta_{ij} - k_i k_j/k^2)E(k)$, where $E(k)$ is the modal spectrum with $E(k) = Ck^{-\alpha}$ in the inertial range; $\alpha = \frac{5}{3} + 2$ for Kolmogorov scaling (see appendix A). Unfortunately, modal spectra are often not experimentally available, with researchers having to make do with the reduced spectra. (This is also the case for most single spacecraft solar wind datasets.) The reduced spectral tensor relative to the x direction is defined as $S_{ij}^{\rm red}(k_x) = \iint S_{ij}(\boldsymbol{k})\,{\rm d}k_y\,{\rm d}k_z$, and it is straightforward to show that for k_x in the (powerlaw) inertial range, the ratio of reduced spectral amplitudes is anisotropic,

$$\frac{S_{yy}^{\rm red}(k_x)}{S_{xx}^{\rm red}(k_x)} = \frac{\alpha - 1}{2} \tag{2.3}$$

(the k_x dependence has cancelled out). This is 4/3 for Kolmogorov scaling. Similarly, variances calculated using only contributions from inertial range (and smaller) scales are also misleadingly anisotropic. For instance, if we define $v_y^2(k_x) = 2\int_{k_x}^{\infty} S_{yy}^{\rm red}(k_x')\,{\rm d}k_x'$, etc., with the parameter k_x in the inertial range, then it follows from the same assumptions leading to equation (2.3) that $v_y^2(k_x)/v_x^2(k_x) = (\alpha - 1)/2$. So, somewhat counter-intuitively, a measured variance anisotropy does *not* necessarily imply anisotropy of the modal energy spectrum. (Variance isotropy is recovered when $k_x L_{\rm cor} \ll 1$, i.e. when the $v_j^2(k_x)$ integrals include all scales with significant energy.) Similar results can be derived for isotropic MHD and axisymmetric MHD [19–21].

The above-mentioned calculations assume that the energy spectrum is accurately known. When averaging intervals are less than a correlation scale, the system is likely to be statistically/ergodically undersampled so that the estimate for the spectrum may involve random anisotropies owing to non-convergence [22]. Unravelling these stochastic anisotropies from 'kinematic' ones like those of equation (2.3) and/or genuine physical anisotropies could be very difficult. Moreover, locally computed anisotropy, even when adequately sampled, may be properly viewed as higher-order statistics [23].

When the energy distribution at a given scale, say l, is not isotropic, one speaks of *spectral* (also known as wavevector or correlation) anisotropy. In terms of a modal energy spectrum $E(k_x, k_y, k_\parallel)$, where $\boldsymbol{k} = (k_x, k_y, k_\parallel)$ is the Fourier wavevector, spectral anisotropy might take the form $E(k, 0, 0) \gg E(0, 0, k)$, for example, where $k \sim 1/l$. Equivalently, considering a homogeneous correlation like $R(\boldsymbol{r}) = \langle \boldsymbol{b}(\boldsymbol{x}) \cdot \boldsymbol{b}(\boldsymbol{x} + \boldsymbol{r})\rangle$, the existence of correlation anisotropy would mean that $R(r\hat{\boldsymbol{e}}_1) \neq R(r\hat{\boldsymbol{e}}_2)$, for some independent directions $\hat{\boldsymbol{e}}_1, \hat{\boldsymbol{e}}_2$. Naturally, spectral anisotropy is often associated with energy transfer that is also anisotropic. In particular, for incompressible MHD, there is abundant evidence that strong (and even moderate) mean magnetic fields engender significant suppression of energy transfer in the parallel direction, so that the perpendicular energy cascade is much stronger than the parallel cascade. Note that spectral anisotropy usually occurs over a range of scales, rather than at (isolated) individual scales.

It is useful to elucidate the different kinematic origins of spectral anisotropy and variance anisotropy. We make use of the vector potential for the magnetic fluctuations, defined by $\boldsymbol{b} = \nabla \times \boldsymbol{a}$. Solenoidality of $\boldsymbol{b}$ means that in Fourier space there are only two linearly independent components to $\boldsymbol{a}(\boldsymbol{k})$, at each wavevector $\boldsymbol{k}$, where $\boldsymbol{a}(\boldsymbol{k})$ is the Fourier transform of $\boldsymbol{a}(\boldsymbol{x})$. Choosing $\hat{\boldsymbol{z}} \parallel \boldsymbol{B}_0$ as the reference direction, a toroidal–poloidal decomposition for $\boldsymbol{b}(\boldsymbol{k})$ is

$$\boldsymbol{b}(\boldsymbol{k}) = i\boldsymbol{k} \times \hat{\boldsymbol{z}} a_{\rm T}(\boldsymbol{k}) - \hat{\boldsymbol{k}} \times (\boldsymbol{k} \times \hat{\boldsymbol{z}}) a_{\rm P}(\boldsymbol{k}), \tag{2.4}$$

provided $\boldsymbol{k} \times \hat{\boldsymbol{z}} \neq \boldsymbol{0}$.[1] This decomposition is general and in no way assumes that the fluctuations are waves (linear or otherwise). Nonetheless, in cases where linear MHD waves are present, the two potentials are associated rather cleanly with the different types of waves. The toroidal piece of $\boldsymbol{b}$, proportional to $a_{\mathrm{T}}(\boldsymbol{k})$, is polarized in the same sense as an Alfvén wave's $\boldsymbol{b}$, whereas magnetosonic waves have their $\boldsymbol{b}$ polarized in the same sense as the $a_{\mathrm{P}}(\boldsymbol{k})$ contributions. In the incompressible limit, $\boldsymbol{v}$ may be decomposed exactly as above, while in the compressible case, a component of $\boldsymbol{v}$ parallel to $\boldsymbol{k}$ must also be allowed for.

Assuming axisymmetry about $\boldsymbol{B}_0$, variance anisotropy is determined by the relative magnitudes of the potentials a_{T} and a_{P}. For instance, if $a_{\mathrm{P}}(\boldsymbol{k}) = 0$ for all wavevectors, then $b_z(\boldsymbol{x}) = 0$ identically, yielding an extreme case of variance anisotropy (a superposition of Alfvén waves would have this configuration). Spectral anisotropy, on the other hand, is determined by how the potentials vary with the direction of $\boldsymbol{k}$. For example, how $a_{\mathrm{T}}(5, 0, 0)$ differs from $a_{\mathrm{T}}(3, 0, 4)$, where these both produce a $b_y(\boldsymbol{k})$.

Note that the connection between variance anisotropy (related to the minimum variance direction, MVD) and spectral anisotropy is not unique. Hence, variance anisotropy information—on its own—is usually not sufficient to infer the actual spectral anisotropy. A well-known example involving two-dimensional turbulence and slab Alfvén waves illustrates this. Turbulence that is strictly two-dimensional (with respect to the z-axis) has $a_{\mathrm{P}}(\boldsymbol{k}) = 0 = b_z(\boldsymbol{x})$ and a toroidal potential that is independent of $k_\parallel$: $a_{\mathrm{T}}(k_x, k_y)$. Its MVD is in the z-direction. Slab Alfvén waves also have $a_{\mathrm{P}} = b_z = 0$ and are polarized in the x–y plane. Thus, a superposition of them will have an MVD in the z-direction—just as two-dimensional turbulence does. However, the wavevector dependence of the slab waves is completely complementary to that of two-dimensional turbulence because they have $a_{\mathrm{T}} = a_{\mathrm{T}}(k_\parallel)$. Clearly, an MVD analysis cannot discriminate between these physically very different states. Recall, also, that the amplitude of a linear Alfvén wave with wavevector $\boldsymbol{k}$ is in the $\boldsymbol{k} \times \boldsymbol{B}_0$ direction, so that the MVD is itself not unique here. That is, all directions in the $\boldsymbol{k}$–$\boldsymbol{B}_0$ plane serve as MVDs for a non-slab Alfvén wave.

3. Spectral anisotropy

Measurements in laboratory plasma physics devices provided the first indications of the prevalence of spectral anisotropy for systems with an energetically significant mean magnetic field, $\boldsymbol{B}_0 = B_0\hat{\boldsymbol{z}}$ [24,25]. In these studies, correlation lengths parallel to $\boldsymbol{B}_0$ were found to be much larger than those in directions perpendicular to $\boldsymbol{B}_0$, indicating that at smaller scales energy is mostly associated with perpendicular structure. Physical grounds for this behaviour were presented [26,27], and Shebalin *et al.* [28] provided an explanation based on 'weak MHD turbulence' and the associated suppression of parallel spectral transfer. Later, Goldreich & Sridhar [29,30] proposed a strong turbulence ('critical balance', CB) phenomenology that accounts for the anisotropy, and this and its cousins are widely used in current modelling approaches to MHD turbulence. The derivation of reduced MHD (RMHD) owing to Montgomery [26,27] also makes it clear how this anisotropy arises in a strong turbulence context: the strongest turbulence occurs when nonlinearity operates more quickly than Alfvén wave propagation. This provides the small parameter for deriving RMHD. The theory breaks down if there is too much parallel spectral transfer; however, the argument of Shebalin *et al.* [28] shows that such transfer is inhibited. Recently, an analytic explanation that is neither perturbative nor phenomenological was advanced [31]. These explanations are reviewed in §3b.

In the solar wind, an early report of correlation anisotropy was provided by Crooker *et al.* [32], using 1 AU magnetic field data from ISEE 1 and ISEE 3. Calculations of a hybrid correlation coefficient between the data from the two spacecraft revealed the presence of anisotropic magnetic features, with parallel scale lengths at least four times the perpendicular ones. Some years later, a two-dimensional correlation function for the magnetic field was constructed, $R(r_\perp, r_\parallel)$,

[1]'Slab' modes, i.e. Fourier modes $\boldsymbol{v}(\boldsymbol{k})$ and $\boldsymbol{b}(\boldsymbol{k})$ with their $\boldsymbol{k}$ parallel to $\hat{\boldsymbol{z}}$, need to be handled separately. For example, as $\boldsymbol{b}(k_\perp = 0, k_z) = \hat{\boldsymbol{x}}a_x(k_z) + \hat{\boldsymbol{y}}a_y(k_z)$.

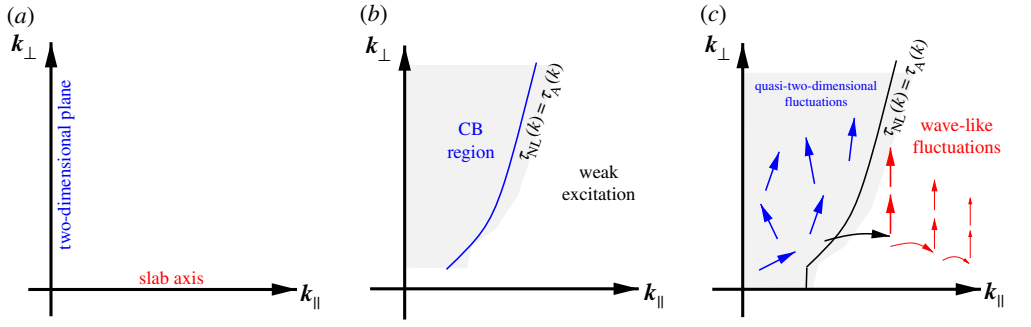

Figure 1. Fourier space regions associated with MHD turbulence models and phenomenologies. (*a*) Slab + 2D. (*b*) Critical balance and the equal time-scale curve. (*c*) Quasi-two-dimensional fluctuations + wave-like fluctuations, with the arrows indicating typical directions of spectral energy transfer; transfer within and between regions involves at least somewhat different physics. (Online version in colour.)

using 1 AU data [33]. This too indicated that the magnetic energy distribution was anisotropic, with contours of $R(r_\perp, r_\parallel)$ displaying a 'Maltese cross'-type pattern with power enhancements approximately parallel to and perpendicular to the mean magnetic field. These results suggested that *two-component* models for the fluctuations might be of use.

The many subsequent observational studies have added quantitative details and are, on the whole, in broad agreement with each other. At MHD scales, results from nonlinear simulations are often in accord with the solar wind observations. Below the proton gyroscales, there is still much debate as to whether the important physics is due to particular wave modes, turbulence and cascades, or some combination of these.

Several useful idealizations or phenomenologies for the observed spectral anisotropy exist, and we now describe two of them. The first is a two-component 'slab + 2D' model [33], for which excited wavevector modes have either $\boldsymbol{k} = k_\parallel \hat{\boldsymbol{B}}_0$ (the slab piece) or $\boldsymbol{k} \cdot \boldsymbol{B}_0 = 0$ (the two-dimensional piece; figure 1*a*). The modal energy spectrum is then $E(\boldsymbol{k}) = E_{\rm slab}(k_\parallel)\delta(k_x)\delta(k_y) + E_{\rm 2D}(k_x, k_y)\delta(k_\parallel)$. For incompressible fluctuations, the slab fluctuations are strictly transverse to $\boldsymbol{B}_0$, whereas the two-dimensional ones could be so-called 2.5D meaning that they can have an amplitude component parallel to $\boldsymbol{B}_0$. Usually, we will not need to distinguish between slab+2D and slab + 2.5D. Further assumptions can be imposed, e.g. axisymmetry with respect to the $\boldsymbol{B}_0$ axis and/or powerlaw inertial ranges. Note that this slab + 2D model does not make any inherent assumptions about the specific nature of the fluctuations, only about the wavevector dependence of each piece. That said, Alfvén waves and two-dimensional turbulence are well-motivated candidates for the slab and two-dimensional components, respectively. When dissipation range scales are considered, kinetic Alfvén waves (KAWs) are another candidate for the two-dimensional piece.

Clearly slab + 2D is a rather drastic approximation, with excitations restricted to modes either on the $k_\parallel$ axis or in the $k_\parallel = 0$ plane. Thus, most of $\boldsymbol{k}$-space is unpopulated and it seems likely this is an oversimplification. Nonetheless, such idealized skeleton models provide attractive analytic tractability and, perhaps surprisingly, have enjoyed some success in matching observations, suggesting that they often capture the important elements of the situation.

A class of inertial range models with more realistic coverage of $\boldsymbol{k}$-space than slab + 2D is the set of phenomenologies based on CB ideas [29,30]. In these, the energy is concentrated in wavevector modes for which the linear wave time scale $\tau_{\rm A}(\boldsymbol{k})$ is comparable to the nonlinear time scale $\tau_{\rm nl}(\boldsymbol{k})$ (figure 1*b*). For MHD, the anisotropic nature of $\tau_{\rm A}(\boldsymbol{k}) = 1/|k_\parallel B_0|$, along with the assumption of isotropic forcing at scales of order $L_{\rm cor}$ (the energy-containing scale for the turbulence) leads to the *equal time-scale* curve $k_\parallel B_0 \sim (u_0/L_{\rm cor})(kL_{\rm cor})^{2/3}$, where u_0 is the RMS turbulence velocity.[2] The key

[2]Boldyrev [34,35] has shown that if there is also a scale-dependent alignment of $\boldsymbol{v}$ and $\boldsymbol{b}$ fluctuations, the nonlinear time scale is weakened, leading to a different scaling for the equal time-scale curve, e.g. $k_\parallel \sim k_\perp^{1/2}$.

point is that modes with $\boldsymbol{k}$s 'near' the equal time-scale curve have important nonlinear physics, whereas modes with $\boldsymbol{k}$s well outside the curve may have some prominent wavelike physics, because $\tau_{\rm nl}(\boldsymbol{k}) \gg \tau_{\rm A}(\boldsymbol{k})$ there. The width of the CB region around the equal time-scale curve is not fully determined by the phenomenology and various models for it have been employed [29,36,37]. Note that CB does not require wavevector modes with $k_\parallel \gg k_\perp$ (e.g. slab-like modes) to be unpopulated, although their energy level is assumed to be low. Many implementations of CB treat this component as negligible, despite its importance in applications such as scattering of cosmic rays [38,39]. Around the equal time-scale curve, the Alfvén wave time scale plays a pivotal role. However, any waves at these $\boldsymbol{k}$s are argued to only last for one or so periods and thus are rather fleeting things [29]. The extent to which wave properties like dispersion relations and eigenstructure are important in turbulence is still under investigation [11,40–42]. Figure 1*c* indicates typical directions of spectral energy transfer inside and outside the equal time-scale curve (cf. [3]).

(a) Review of observations

Following the original demonstration of correlation anisotropy [33], many examples of two-dimensional correlation functions, e.g. $R(r_\perp, r_\parallel)$, two-dimensional structure functions, and two-dimensional spectra have been presented. Here, $r_\perp$ and $r_\parallel$ are relative to the mean field $\boldsymbol{B}_0$, and similarly for $k_\perp$ and $k_\parallel$. Regrettably, it is not completely straightforward to compare results from these studies, because they may employ distinct techniques, single or multiple spacecraft, and/or pertain to different scale ranges. Table 1 lists results and some relevant parameters from many of these studies, and we discuss a selection of them below.

Using 5 years of near-Earth (ACE) data, Dasso *et al.* [52] investigated correlation anisotropy for scales around the middle decade of the inertial range. It was found that fast wind ($U_{\rm sw} > 500\,{\rm km\,s^{-1}}$) was relatively more dominated by fluctuations with quasi-parallel $\boldsymbol{k}$, whereas for slow wind ($U_{\rm sw} < 400\,{\rm km\,s^{-1}}$), the quasi-perpendicular modes were more dominant. As slow wind takes longer to get to 1 AU, this can be interpreted as meaning its turbulence has had more time to evolve, in this case, towards an energy distribution concentrated in quasi-perpendicular $\boldsymbol{k}$s. Intriguingly, at somewhat smaller scales than Dasso *et al.* studied, results from the 'spectrum ratio' test (see below) indicate very little wind speed or distance (over 0.3–0.9 AU) dependence to the spectral anisotropy [45,46]. Hamilton *et al.* suggest that at smaller scales the turbulence may already be in approximate steady state by 0.3 AU, whereas at larger scales [52], the distinct anisotropies seen in fast and slow wind may be a remnant of the solar source of the fluctuations.

Wicks *et al.* [53] calculated magnetic energy (wavelet) spectra using Ulysses data. They report that the power is roughly isotropic for scales larger than inertial range ones, $k\rho_{\rm i} \lesssim 3 \times 10^{-3}$. At larger wavenumbers, anisotropy consistent with more power in oblique wavevectors is present and its strength increases as $k\rho_{\rm i}$ increases, until $k\rho_{\rm i} \approx 0.5$ is reached.

The above results are consistent with the perpendicular energy cascade rate being greater than the parallel one, as is also seen in direct 1 AU measurements of the cascade rate, via third-order moment calculations [8,54]. Simulation results [3,28,36,55,56] and phenomenologies [29,35,57,58] support the notion that small scales are more anisotropic, and achieve their quasi-two-dimensional-type states more rapidly than larger scales.

A related method of investigating spectral anisotropy was proposed by Bieber *et al.* [19]. When the fluctuations are modelled as slab + 2D, the frequency spectrum exhibits a dependence on ψ—the angle between $\boldsymbol{B}_0$ and the mean solar wind speed $\boldsymbol{U}$—that can be used to estimate the fraction of energy in the slab and two-dimensional components. Assuming powerlaw slopes, α, for each component, one obtains

$$fP(f,\psi) = 2C_{\rm slab}\left(\frac{2\pi f}{U_{\rm sw}\cos\psi}\right)^{1-\alpha_{\rm slab}} + 2C_{\rm 2D}\left(\frac{2\pi f}{U_{\rm sw}\sin\psi}\right)^{1-\alpha_{\rm 2D}}, \tag{3.1}$$

Table 1. Observational results from slab + 2D fits to magnetic spectra, as first used by Bieber *et al.* [19]. Slow wind is generally $U_{sw} < 400$ km s^{-1} and fast wind $U_{sw} > 500$ km s^{-1}. Frequencies above ≈ 0.3 Hz are treated as being in the dissipation range. The dissipation range typically extends to much higher frequencies than the ≈ 1 Hz attainable in the cited studies. Measurements are from the ecliptic unless 'wind type' column notes otherwise. 'IR' indicates frequencies are in the inertial range and 'diss' that they are in the dissipation range. IR results usually show a dominance of two-dimensional (i.e. quasi-$k_\perp$) energy (an exception is the slow wind ahead of co-rotating interaction regions, CIRs), whereas in the dissipation range the slab component is more likely to be predominant.

wind type	distance (AU)	2D%	freq. range (Hz)	comments	reference
mixed	0.3–1	74	0.001–0.02	Helios. 454 spectra	[19]
mixed	1	89	0.01–0.2	Wind, 33 intervals	[43]
		54	0.5–1.5		
fast, high lat	2–3.5	56	IR	Ulysses. Preliminary results	[44]
mixed, low/high lat	3.4–5	70–80			
mixed	1	68	0.008–0.1	ACE, 567 samples	[45]
		26	0.3–0.8		
fast		50	IR	101 samples	
		34	diss		
slow		78	IR	234 samples	
		16	diss		
mixed	0.3–1	73	0.005–0.02	Helios. No distance or	[46]
fast		67		speed dependence within	
slow		84		errors	
mixed	1	62	0.008–0.1	ACE. 66 $\beta_p > 1$ intervals	[47]
		32	0.3–0.8		
fast, high lat	1.4	92	0.004–0.2	Ulysses. Wavelets, $\boldsymbol{B}_0^{loc}$	[48]
slow	1	70–100	$\sim 10^4$ km	Cluster. Structure functions	[49,50]
intermediate		50–85			
fast (behind CIR)	1	80	0.008–0.2	ACE. 5 CIRs and the	[51]
		45	0.4–0.8	fast/slow wind either side	
CIR		99	IR		
		61	diss		
slow (front CIR)		44	IR		
		0	diss		

where C_{2D} and C_{slab} are the fitting parameters. Using Helios data (0.3–1 AU), they found a best-fit value of 95% two-dimensional, 5% slab, for a frequency band in the inertial range. Bieber *et al.* also proposed the 'spectrum ratio' test, which makes (separate) use of the diagonal components of the spectral matrix, rather than the trace employed in equation (3.1). For this test, the best-fit value was 84% two-dimensional, 16% slab. Both tests strongly support the conclusion that fluctuation energy is mostly in Fourier modes with their wavevectors $\boldsymbol{k}$ perpendicular to the mean field $\boldsymbol{B}_0$.

The 'spectrum ratio' test has since been employed on many other solar wind intervals [43,45–47,51,59] (table 1). Inertial range results are mostly consistent with an energetic predominance for two-dimensional modes, with the two-dimensional fraction ranging from

50% to ≈100%. Moreover, in the inner heliosphere, there is only weak distance or wind speed dependence in the results, at least towards the high-frequency end of the inertial range [45,46].

Slab + 2D-type fits similar to equation (3.1) have been widely used [48–50,53,60–62] and these also report high values for the inertial range two-dimensional fraction, e.g. 70–100%. Interestingly, Forman *et al.* [62] compared slab + 2.5D fits and CB fits for Ulysses inertial range data, finding that both produce good agreement with the observations, although the CB fits are a little better.

He *et al.* [63] investigate the radial evolution of inertial range spectral anisotropy using Helios data (0.3–0.87 AU). They report two-dimensional energy spectra that exhibit enhanced power along a ridge at $k_\perp > k_\parallel$, roughly similar to a CB scaling. Another power enhancement exists close to the $k_\parallel$ axis, suggestive of a slab component. At larger distances, the ridge is more oblique and the slab-like component weaker. These results are obtained using a method, new to the community, that involves fitting of processed data at an intermediate stage. First, the observations are used to calculate a two-dimensional $(r_\perp, r_\parallel)$ correlation function, with its arguments relative to local mean fields $\boldsymbol{B}_0^{\mathrm{loc}}$. Second, a direction θ_k is chosen, and the two-dimensional function integrated over the coordinate normal to that direction to give a one-dimensional (projected) correlation function. This is done for many different θ_k. Third, stretched exponentials are fitted to each of these one-dimensional projections (to ensure their Fourier transforms are positive), and then these two-dimensional fits are Fourier transformed and reassembled using their θ_k to give the three-dimensional spectrum. Further calibration of this procedure on known (synthetic) two-dimensional spectra would be welcome.

We turn now to the dissipation range (frequencies above $\sim f_{\mathrm{ci}}$), where spectral anisotropy observations are a little puzzling. When the spectrum ratio test is employed, the usual finding is that slab fluctuations are energetically dominant. See the rows in table 1 with either 'diss' or a minimum frequency of 0.3 Hz in the 'freq. range' column. Note that in all cases where both inertial range and dissipation range scales were investigated as part of the same study, the two-dimensional fraction for the dissipation range is substantially smaller than that for the inertial range, and usually less than 50%. A possible explanation is that the two-dimensional component is preferentially dissipated and associated with a steepened spectrum at those scales [43,53,64]. Another possibility is that temperature anisotropy instabilities excite whistlers and/or ion cyclotron waves at quasi-parallel wavevectors with $k_\parallel d_{\mathrm{i}} \approx 1$, leading to increased dissipation range energy for the slab-like component [9,65,66].

However, the situation is complicated, as shown, for example, by Podesta [60]. Using STEREO data and a wavelet-based approach (with local mean fields), Podesta determined the fluctuation power at different angles ψ between the solar wind velocity and $\boldsymbol{B}_0^{\mathrm{loc}}$. Here, we are interested in the power in the angle band near 90° (the quasi-$k_\perp$ power), and that near 0° (the quasi-$k_\parallel$ power). Their ratio, $P(f;\psi \approx 90°)/P(f;\psi \approx 0°) = P_\perp/P_\parallel$, is a measure of the dominance of quasi-$k_\perp$ power over quasi-$k_\parallel$ power. An example from [60] is reproduced here as figure 2*a*. The dissipation range behaviour is interesting: first the spectral anisotropy decreases, then increases to a significant (absolute) maximum for the evaluated scales, at ≈1 Hz, and then decreases sharply to its lowest dissipation range value. At all frequencies shown, the quasi-$k_\perp$ power is dominant, which differs from the typical dissipation range results listed in table 1, although the trend at higher f is towards reduced dominance. Podesta attributes the initial dissipation range decrease of $P_\perp/P_\parallel$ to an enhanced population of nearly parallel-propagating waves at $k_\parallel \rho_{\mathrm{i}} \sim 1$, owing to an unknown source, and the peak to a strong perpendicular cascade at those f. Results from eight other intervals examined by Podesta [60] are similar.

Other studies, including those employing the multi-spacecraft k-filtering technique [68,69], have also found that the quasi-perpendicular wavevectors remain energetically dominant in the dissipation range [67,70–75], as in the inertial range. In k-filtering, multi-spacecraft observations (e.g. from Cluster) are used to construct the spectral energy density as a function of $\boldsymbol{k} = (k_x, k_y, k_z)$ and spacecraft frame frequency, ω_{sc}. Then, at each ω_{sc}, peaks in the energy density are sought and the associated $\boldsymbol{k}$s employed, with the Doppler shift $\boldsymbol{k} \cdot \boldsymbol{U}$, to determine the frequencies in the plasma rest frame, and hence points on dispersion relations. Energy not associated with ω_{sc}–$\boldsymbol{k}$ peaks is apparently not usually considered further, or is treated as incoherent noise ([69,74]). The

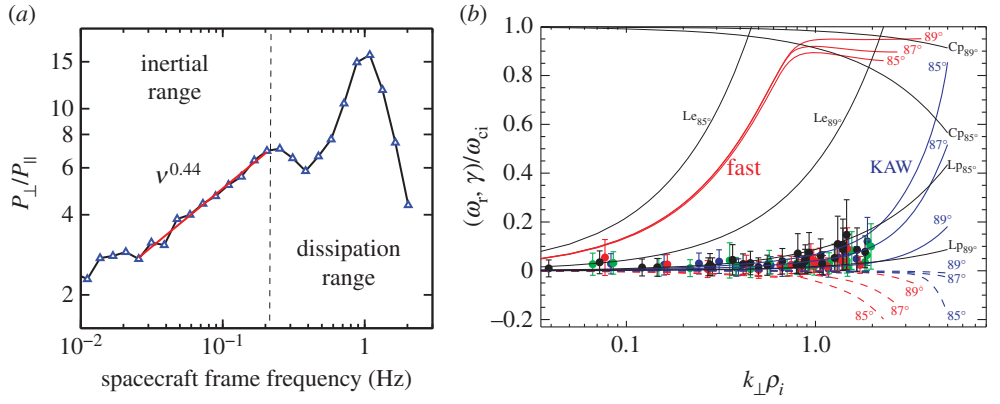

Figure 2. (*a*) Wavevector anisotropy from 1 AU study by Podesta [60]. $P_\perp$ and $P_\parallel$ are the reduced magnetic spectra in angular bins close to the $k_\perp$ and $k_\parallel$ axes. Copyright AAS. Reproduced with permission. (*b*) Observational (1 AU) frequency–wavenumber pairs (circles) and linear theory dispersion relations for KAWs and fast modes with wavevectors at the stated angles (solid curves). Dashed curves are associated linear theory damping rates, γ. Highly oblique KAWs are not inconsistent with the data, but the data are also consistent with low-frequency quasi-two-dimensional turbulence. Reprinted with permission from Sahraoui *et al.* [67]. Copyright 2010 © American Physical Society. (Online version in colour.)

method avoids using the Taylor frozen-flow approximation (appendix A), and thus can provide more direct information on spatial structure.

Figure 2*b*, reproduced from Sahraoui *et al.* [67], presents some *k*-filtering results from Cluster, finding $\omega \lesssim \Omega_{ci}/10$ when $0.05 < k_\perp d_i \lesssim 2$, where ω is the plasma frame Fourier frequency. Although this is consistent with linear Maxwell–Vlasov dispersion relations for very oblique KAWs ($\theta_{kB_0} = \cos(\hat{\boldsymbol{k}} \cdot \hat{\boldsymbol{B}}_0) \approx 88^\circ$), with such strong obliquities of the $\boldsymbol{k}$s the results can also be interpreted as indicating the presence of relatively energetic quasi-two-dimensional turbulence. Indeed, Narita *et al.* [71,72,76,77] use essentially the same multi-spacecraft technique, over similar wavenumber ranges, and state that they find no evidence of a linear dispersion relation. They favour an explanation in terms of well-developed strong quasi-two-dimensional turbulence.

Recently, two-component and/or CB energy spectrum models have been employed to determine the associated normalized reduced magnetic helicity spectra, σ_m, as a function of time scale and ψ, the angle between the solar wind and $\boldsymbol{B}_0^{\mathrm{loc}}$ [66,78]. These are compared with observational determinations of σ_m, in efforts to constrain the free parameters of the energy spectra models. The scales investigated are mostly in the inertial range but, as in many of the studies discussed above, the beginning of the dissipation range is also sampled. The best fits are obtained when the bulk of the energy is in quasi-$k_\perp$ modes.

Summarizing the dissipation range results, those obtained using the 'spectrum ratio'-type tests usually indicate a preponderance of quasi-$k_\parallel$ power, whereas most studies employing other techniques find the quasi-$k_\perp$ power is dominant. A resolution of this discrepancy would be welcome. Other recent reviews have further discussion of dissipation range anisotropy [4,6]. Given the disparate results from the various types of studies, it is evident that further work is needed.

Finally, we note that cosmic ray scattering data also provide support for spectral anisotropy. Models for the scattering based on slab waves show poor agreement with observations, whereas slab+2D-type models display much better agreement [19,38,39,79–81].

(b) Theoretical explanations

Let us sketch the weak turbulence argument for the development of spectral anisotropy and enhanced perpendicular energy transfer in incompressible MHD [28] (see also [82–85]). The primary assumption is that at leading order the fluctuations are *Alfvénic*, meaning that at each

point in space either $\boldsymbol{v}(\boldsymbol{x},t)=\pm\boldsymbol{b}(\boldsymbol{x},t)$, or there is a superposition of these two states. Equivalently, in Fourier space, for (inertial range) wavevectors $\boldsymbol{k}$, one has $\boldsymbol{v}(\boldsymbol{k},t)=\pm\boldsymbol{b}(\boldsymbol{k},t)$, or a superposition of these two states. In the absence of nonlinear effects, such fluctuations are propagating (shear) Alfvén waves with frequencies $\omega(\boldsymbol{k})=\pm\boldsymbol{k}\cdot\boldsymbol{B}_0$, provided $\boldsymbol{k}\cdot\boldsymbol{B}_0\neq 0$. The waves with a group velocity ($\boldsymbol{v}_g=\nabla_{\boldsymbol{k}}\omega$) parallel to $\boldsymbol{B}_0$ have $\omega(\boldsymbol{k})=\boldsymbol{k}\cdot\boldsymbol{B}_0$,[3] whereas those with an antiparallel group velocity have $\omega(\boldsymbol{k})=-\boldsymbol{k}\cdot\boldsymbol{B}_0$. However, two-dimensional fluctuations—those with $\boldsymbol{k}\cdot\boldsymbol{B}_0=0$—are *not* linear Alfvén waves and they do not propagate along $\boldsymbol{B}_0$. When their nonlinear self-interactions are strong, they are the elements of two-dimensional turbulence. In 'wave language', they may be called non-propagating modes or vortex modes. Whatever they are called, they play a crucial role in the argument.

The next step is to use the leading-order Alfvénic fluctuations to calculate the first-order nonlinear corrections. Recall that for incompressible three-dimensional MHD, $\partial z^-/\partial t=-z^+\cdot\nabla z^-+\cdots$, with an analogous equation for z^+. This Elsasser form highlights the key point that nonlinear interactions only occur if both z^+ and z^- are non-zero. Now, consider the interaction of Fourier modes $z^+(\boldsymbol{k}')$ and $z^-(\boldsymbol{k}'')$, with respective frequencies $\omega(\boldsymbol{k}')=-\boldsymbol{k}'\cdot\boldsymbol{B}_0$ and $\omega(\boldsymbol{k}'')=\boldsymbol{k}''\cdot\boldsymbol{B}_0$. These will combine to drive $z^-(\boldsymbol{k})$ which has frequency $\omega(\boldsymbol{k})=\boldsymbol{k}\cdot\boldsymbol{B}_0$—if the well-known matching (resonance) conditions for the wavevectors and frequencies are satisfied: $\boldsymbol{k}=\boldsymbol{k}'+\boldsymbol{k}''$ and $\omega(\boldsymbol{k})=\omega(\boldsymbol{k}')+\omega(\boldsymbol{k}'')$. Dotting the former with $\boldsymbol{B}_0$ and using the equations for the frequencies yields

$$k_\parallel=k'_\parallel+k''_\parallel\quad\text{(quadratic nonlinearity)}\tag{3.2}$$

and

$$k_\parallel=-k'_\parallel+k''_\parallel\quad\text{(frequency matching)}.\tag{3.3}$$

Clearly, these can both be true only if $k'_\parallel=0$, i.e. $z^+(\boldsymbol{k}')$ is a two-dimensional mode.[4] Physically, this can be interpreted as two Alfvén waves with the same $k_\parallel$ and frequency, propagating through a 'two-dimensional structure'.[5] The two-dimensional structure enables the transfer of energy from one wave to the other, necessarily at constant $k_\parallel$, so that it is the perpendicular structure of the waves that alters. Assuming approximate locality of the Fourier space interactions, i.e. $\boldsymbol{k}'_\perp\sim\boldsymbol{k}''_\perp$, means that typically $|\boldsymbol{k}_\perp|\gtrsim|\boldsymbol{k}''_\perp|$ and the net energy transfer will tend to be towards larger $\boldsymbol{k}_\perp$: a forward cascade in the $k_\perp$ plane. Because, at this order, no energy is transferred in the parallel direction, it is evident that the energy spectrum will become anisotropic. In essence, this is an argument about how fluctuations that retain a strong wave-like character (i.e. are non-two-dimensional) evolve. Details of the formal application of weak turbulence theory are available [84,85], including a derivation of the associated powerlaw slopes for the energy spectra. For the zero cross helicity case, the inertial range energy spectra scale as $k_\perp^{-2}$, with the $k_\parallel$ dependence set by the driving and/or initial conditions (ICs).

Gary [86] has presented a similar analysis for modes in linear Vlasov–Maxwellian plasmas with $\beta_p=0.01$–1. Assuming a two-dimensional (radial) k-space cascade, and the interaction of either three Alfvén modes, three magnetosonic modes (both at MHD scales: $kd_i<0.5$) or three magnetosonic-whistler modes ($0.4<kd_i<4$) he generally finds that the cascade leads to energetic predominance for $k_\perp>k_\parallel$. The exception is the $\beta_p=1$ magnetosonic mode cascade, which seems to favour $k_\perp\approx k_\parallel$. One conclusion is that there appear to be no cases in which an enhanced parallel cascade occurs.

Although this weak turbulence approach—nonlinear corrections to the linear wave dynamics—appears plausible for systems with low levels of nonlinear activity, it is striking, and intriguing, that spectral anisotropy is also a well-observed feature in numerical simulations of *strong* MHD turbulence, that is, in systems where the nonlinear effects are strong, rather than perturbative [28,36,55,83,87–90]. A strong turbulence explanation is needed.

[3]Since then $\exp(i[k_\parallel z-\omega(\boldsymbol{k})t])\rightarrow\exp(ik_\parallel[z-B_0t])$, which has the correct sense of propagation. Note that $k_\parallel=\boldsymbol{k}\cdot\hat{\boldsymbol{B}}_0$ may be positive or negative.

[4]The special case where all three of $\boldsymbol{k}$, $\boldsymbol{k}'$ and $\boldsymbol{k}''$ are perpendicular to $\boldsymbol{B}_0$, giving a purely two-dimensional interaction, is sometimes referred to as the 'trivially resonant' case.

[5]See [84] for a Bragg scattering analogy.

One possibility is that even in strong turbulence, the fluctuations retain some wavelike characteristics, such as time scale, eigenstructure or polarization for the mode. CB phenomenologies include such assumptions, as does the recently posited *quasi-linear premise* which states that 'some properties of magnetized plasma turbulence can be understood by modelling the turbulence as a collection of randomly phased linear waves' [42], the idea being that the nonlinear interactions transfer energy between linear wave modes, with the latter in some sense dominant, because they retain (at least some) linear wave characteristics. In particular, it is argued that for 'a turbulent fluctuation with a given wavevector, the amplitude and phase relationships between different (vector) components of that fluctuation are likely to be related to linear eigenfunctions of the characteristic plasma wave modes'. Numerical and observational evidence for and against this premise is discussed by Klein *et al.* [42], and it is not yet clear whether the premise correctly describes the physics of turbulence. Note that as quasi-linear premise proponents acknowledge, third- and higher-order correlations will probably be incorrect, because the random phase assumption makes it difficult to achieve the appropriate phase correlations inherent in these higher-order correlations. Such correlations are of course essential to the existence of coherent structures, including current sheets. Thus, magnetic reconnection—robustly seen in MHD, hybrid and particle-in-cell simulations, and solar wind and magnetospheric observations—may be difficult to reconcile with the quasi-linear premise (cf. [11]). Note that weak turbulence approaches do not always require random phases [91,92].

We are aware of only one explanation for spectral anisotropy that is neither perturbative nor phenomenological and also allows for strong turbulence [31,93]. It is based on the coupling of third-order (and higher) correlations to the second-order correlations (e.g. the energy spectrum), and we now outline it. Consider the infinite set of two-point correlation functions in homogeneous incompressible MHD, such as $R^{+}_{ij}(\boldsymbol{r},t)=\langle z^{+}_{i}(\boldsymbol{x})z^{+}_{j}(\boldsymbol{x}+\boldsymbol{r})\rangle\equiv\langle z^{+}_{i}z^{+\prime}_{j}\rangle$ and $Q_i(\boldsymbol{r},t)=\langle z^{-\prime}_{i}\boldsymbol{z}^{+}\cdot\boldsymbol{z}^{-\prime}\rangle$, where the prime ($'$) is shorthand for evaluation of the field at position $\boldsymbol{x}+\boldsymbol{r}$, rather than $\boldsymbol{x}$. Their evolution is governed by the unclosed hierarchy of von Kármán–Howarth (vKH) equations [93–97]. We write the first three of these schematically for a generic fluctuation u,

$$\frac{\partial}{\partial t}\langle uu'\rangle=\langle uu'u'\rangle+\nu\langle uu'\rangle, \tag{3.4}$$

$$\frac{\partial}{\partial t}\langle uu'u'\rangle=\langle uuu'u'\rangle+B_{0j}\langle uu'\partial_j u'\rangle+\cdots \tag{3.5}$$

and

$$\frac{\partial}{\partial t}\langle uuu'u'\rangle=\langle uuu'u'u'\rangle+B_{0j}\langle uuu'\partial_j u'\rangle+\cdots. \tag{3.6}$$

Most terms involving pressure and dissipation (e.g. viscosity, ν) are not shown, and the only spatial derivatives indicated are those involving $\boldsymbol{B}_0\cdot\nabla=B_{0j}\partial_j$. (The schematic equations are thus not dimensionally correct. See Wan *et al.* [93] for the full equations.) The vKH equations hold for all homogeneous flows, whether laminar, weakly turbulent or strongly turbulent.

Inspecting the terms in the vKH equations, it is striking that $\boldsymbol{B}_0$ appears in the third-order and all higher-order equations, but not in the second-order one. And yet, simulations, solar wind observations, and theories and phenomenologies all indicate that the mean field exerts considerable influence on second-order correlations, inducing anisotropy in the energy spectrum, for example. This apparent inconsistency is resolved by considering the *coupling* of these equations. Equation (3.5) shows that $\langle uu'u'\rangle$ has an explicit dependence on $\boldsymbol{B}_0$ (and also an implicit one via the dependence of the fourth-order correlation on $\boldsymbol{B}_0$). In particular, its characteristic time scale will be a function of $\boldsymbol{B}_0$, presumably related to the Alfvén time scale for the lag $\boldsymbol{r}$. Hence, the evolution of $\langle uu'\rangle$, equation (3.4), has a hidden, or implicit, dependence on $\boldsymbol{B}_0$ through the third-order correlation, and this produces anisotropy at second order.

Note that this explanation does not assume anything about the nature of the fluctuations (e.g. wave-like or turbulence), except that the correlations are homogeneous. On the other hand, although the *pathway* for the development of second-order correlation anisotropy is clear (with the $\boldsymbol{B}_0$ dependence 'cascading in' from (all) higher orders), the specifics of the process are not apparent. In this sense, we are still seeking a full strong turbulence explanation.

4. Component (variance) anisotropy

This is conveniently quantified using ratios. There are numerous possible choices, many of which have seen use in the literature; however, provided the same averaging procedure is used in each case, it is straightforward to transform between these variants. Here, we employ a mean-field-aligned coordinate system with $\boldsymbol{B}_0$ along the z-axis, and define the *magnetic anisotropy ratio* for fluctuations $\boldsymbol{b} = (b_x, b_y, b_\parallel)$ as

$$A_b = \frac{\langle b_x^2 + b_y^2 \rangle}{\langle b_\parallel^2 \rangle} = \frac{\langle b_\perp^2 \rangle}{\langle b_\parallel^2 \rangle}, \tag{4.1}$$

where $\langle \cdots \rangle$ is an appropriate averaging operator, which might be global or local and carried out in either physical space or Fourier space. In addition, whether $\boldsymbol{B}_0$ is computed as a global or local mean is an important issue [23,48,60,61,98–102]; see appendix B. The velocity anisotropy ratio, A_v, is defined analogously. A popular alternative ratio is the *magnetic compressibility*, $C_\parallel = \langle b_\parallel^2 \rangle / \langle b_\perp^2 + b_\parallel^2 \rangle$, although it is sometimes defined as the square root of this. We remind readers that for averaging intervals shorter than a correlation length or correlation time, $A_b \neq 2$ does *not* necessarily imply that the energy distribution is anisotropic. See the discussion around equation (2.3).

Table 2 summarizes the observational results for A_b, and also A_v in the few cases where it has been reported. Pertinent features of each study include the wind type sampled (e.g. fast, slow, trailing edge of high-speed stream), heliocentric distance and the time scale (or frequency range) over which the fluctuations were averaged to obtain the anisotropy ratios. In many cases, the mean field was calculated as a global average, i.e. over the whole interval. However, in some structure function- or wavelet-based studies, a local mean field $\boldsymbol{B}_0^\mathrm{loc}(\boldsymbol{x})$ is used, and this has been argued to be a more physically motivated approach, because the fluctuations should respond to the local conditions [98,100,101]. Several studies [101,102] indicate that using the global mean field rather than a $\boldsymbol{B}_0^\mathrm{loc}$ typically leads to a larger estimate for $\langle b_\parallel^2 \rangle$, and thus a reduced A_b estimate.

Some trends are evident, although caution should be exercised given the relatively small number of studies listed. First, the dominance of perpendicular power over parallel power is essentially ubiquitous in the inertial range, often by more than a factor of 10. Second, A_b appears to increase with heliocentric distance up to ≈ 1 AU, and decrease thereafter. The data suggest this is the case both at high latitudes (where the wind is almost always fast), and in the ecliptic. Third, $A_b > A_\mathrm{v}$ in both fast wind and slow wind, and from 0.3 to 10 AU. Finally, although not particularly clear from the table, above the proton gyrofrequency $A_b(f)$ decreases (often monotonically) with f towards isotropy. In particular, Kiyani *et al.* [102] report, using 1 AU data, how A_b goes from anisotropic values at MHD scales to isotropic ones as the electron gyroradius is approached (figure 3). An increasing relevance of KAWs is a candidate explanation, and, more generally, they show how the Hall term in Ohm's law causes the parallel variances to increase at sub-ion scales. Other studies report results consistent with this behaviour [43,45,67,108–111].

Perri *et al.* [99] have analysed Cluster data in terms of the eigenstructure of the magnetic variance matrix [103,112] averaged over 13 different time scales from 0.09 to 360 s. They report on the statistics of the ratio of the maximum eigenvalue to the minimum one, Γ, which is related to A_b. Indeed, if the MVD is along the mean field, then $A_b \geq \Gamma$. This is typically the case at large scales in the solar wind, but is not as likely at smaller scales [99], and thus A_b can be less than Γ. Because Perri *et al.* report the *statistics* for Γ and the MVD angle to $\boldsymbol{B}_0^\mathrm{loc}$, it is not straightforward to determine A_b for their data. They find that $\Gamma > 1$ almost always, and that the most probable values are large: $\Gamma \approx 100$ for averaging times of 0.2 s and 1.5 s, and $\Gamma \approx 30$ for 46 s averages. Overall, at both inertial range and dissipation range scales, substantial and scale-dependent MVD-type anisotropy is found. The anisotropy increases at $f > f_\mathrm{ci}$, with the fluctuation amplitude tending to lie in the direction of maximum variance (i.e. be approximately one-dimensional). Note that this is not necessarily inconsistent with the results discussed in the previous paragraph, because as the averaging scale decreases, the MVD tends to lie at a larger angle to the local mean field [99].

Table 2. Anisotropy ratios for the magnetic (and velocity, where available) fluctuations from observational solar wind studies. Data are from the ecliptic unless the 'wind type' column states 'high lat.' 'Mixed' means both fast and slow wind intervals are included. In the time scales column, times indicate the averaging period, whereas frequencies indicate that averaging occurs over frequencies; see original papers for details. The high frequency end of the inertial range is, roughly, the proton gyrofrequency (approx. 0.1 Hz at 1 AU). Essentially, all inertial range cases exhibit 'excess' perpendicular power. Some studies [45–47,59] also show scaling with β_p and relative fluctuation strength.

wind type	distance (AU)	$\frac{\langle b_\perp^2 \rangle}{\langle b_\parallel^2 \rangle}$	$\frac{\langle v_\perp^2 \rangle}{\langle v_\parallel^2 \rangle}$	time scales	comments	reference
fast	0.7–1	8		3 min, 22 min	Mariner 5	[103]
	0.7–1	5		3 h		
trailing edge	0.3	34		3 min	Helios	[104]
	0.9	56				
trailing edge	0.3	13	13	1 h	Helios	[105]
	0.9	19	11			
mixed	1	9	4	1 h	Voyager	[106]
	10	6	4			
fast, high lat	1.7	39		5 min	Ulysses	[107]
	2.4	35				
	3.8	29				
mixed	1	3–53		0.01–0.3 Hz	Wind	[43]
	1	2.4–13		0.5–1.5 Hz		
mixed	0.3–1	1–45		0.01–0.1 Hz	Helios	[46]
fast	1	1–50		0.008–0.01 Hz	ACE	[45,47,59]
	1	1–40		0.3–0.8 Hz		
slow	1	1–100		0.008–0.01 Hz		
	1	0.6–20		0.3–0.8 Hz		
slow	1	5–600		0.02–2 Hz	Cluster	[108]
fast	1	3–20		0.03–4 Hz	Cluster. $\boldsymbol{B}_0^{\mathrm{loc}}$	[101,109]
fast	1	1–19		0.004–60 Hz	Cluster. $\boldsymbol{B}_0^{\mathrm{loc}}$	[102]

Explanations for variance anisotropy in terms of linear wave properties have a seductive simplicity. Numerous authors have used linear kinetic theory to calculate polarizations and other features associated with specific wave modes (e.g. KAWs, whistlers), and then compared these results with observations. Unfortunately, A_b is often insufficient, at least on its own, to make an unambiguous identification of a mode [42,101]. The point has been made that it is important to use the kinetic wave modes, because there are important differences between them and the MHD wave modes [42,101]. For instance, the collisionless Vlasov–Maxwell Alfvén mode has a component along the mean field (finite A_b), whereas the MHD Alfvén mode is polarized strictly transverse to it ($A_b = \infty$). Reasonable agreement between linear theory and observations is used to conclude in favour of one mode or another. The majority of studies cite KAWs as the most likely candidate, with whistlers typically (but not always [64]) being a poor fit to measurements [42,43,64,101,108,109,113,114]. Note that linear theory predictions are overwhelmingly determined using a *uniform and constant global* mean field, whereas recent observational results often employ space (or time)-dependent $\boldsymbol{B}_0^{\mathrm{loc}}$. However, if the direction, say, of $\boldsymbol{B}_0^{\mathrm{loc}}$ varies on a time scale only somewhat slower than that of the fluctuations of interest, then

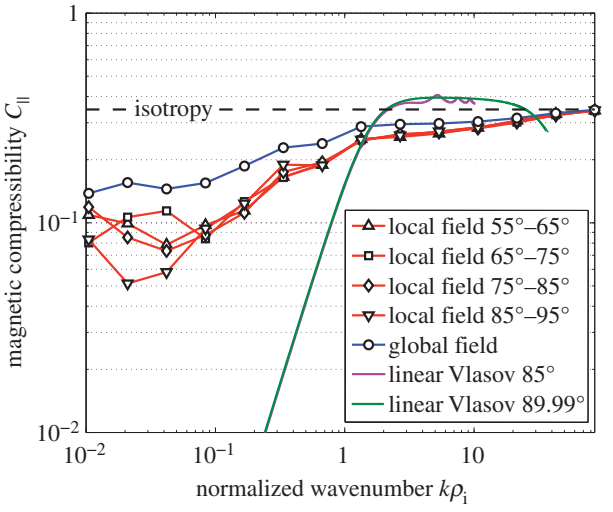

Figure 3. Magnetic compressibility versus wavenumber from a Kiyani *et al.* [102] study at 1 AU. Local mean fields are typically employed, although a comparison with an analysis based on the global field is also shown, along with some linear Vlasov theory results. In the dissipation range, note the tendency towards isotropy with decreasing length scale. Copyright AAS. Reproduced with permission. (Online version in colour.)

$\boldsymbol{B}_0^{\mathrm{loc}}$ is not a very stably defined mean quantity. The relevance of the linear theory results to the observational ones is then unclear. Similar comments apply to the length scale over which $\boldsymbol{B}_0^{\mathrm{loc}}$ is defined [23]. Moreover, these explanations all presume that the fluctuations are dominantly wave-like. Although there is some numerical support for the wave-based explanations of variance anisotropy, for example in particle-in-cell simulations [113] and gyrokinetic simulations [101], it remains unclear whether strong turbulence has this property, at either MHD scales or sub-ion ones [115–117]; cf. §3b.

Another way of analysing variance anisotropy is in terms of the power in the toroidal and poloidal components of the fluctuations (and the longitudinal component for $\boldsymbol{v}$). As stressed in §2, this decomposition is general and does not imply the fluctuations are waves. Nonetheless, the toroidal and poloidal directions do match up cleanly with the polarizations for linearized MHD waves, Alfvén and magnetosonic, respectively. Wicks *et al.* [118] performed such an analysis using Ulysses data. A physical interpretation of their results is that (inertial range) solar wind turbulence mostly consists of toroidal fluctuations that have energy concentrated in quasi-perpendicular wavevectors. The poloidal component is less energetic, for a given $\boldsymbol{k}$, yielding a net elliptical polarization to $\boldsymbol{b}(\boldsymbol{k})$.

To explore this toroidal/poloidal anisotropy further, we present new results from a set of decaying compressible (polytropic) three-dimensional MHD turbulence simulations (see [119] for the equations solved). A periodic pseudospectral method with a resolution of 512 Fourier modes in each Cartesian direction was employed. Figure 4 shows some quantities related to variance anisotropy for three particular runs, each with uniform mean field strength $B_0 = 2$, initial plasma beta $\beta_{\mathrm{p}} = 1$, initial sonic Mach number $M_{\mathrm{s}} = 0.5$, and initially excited wavevectors satisfying $3 \leq |\boldsymbol{k}| \leq 9$. In the column headings, the angle brackets $\langle\cdot\rangle$ denote averaging over the whole simulation domain, and perpendicular and parallel are computed with respect to the global mean field $B_0\hat{\boldsymbol{z}}$. The first column of figure 4 indicates that $A_b > A_{\mathrm{v}}$ (as seen in the solar wind), aside from some early-time transients associated with generation of either longitudinal velocity fluctuations (top two rows) or toroidal and poloidal $\boldsymbol{v}$ (bottom row), depending upon the ICs. From the second column, it appears that when there is some toroidal $\boldsymbol{b}$ present initially, the dynamics acts to make this component $\approx$70–80% of the fluctuation magnetic energy, at least for these particular simulations. The $\boldsymbol{v}$ fluctuations evolve similarly, although their toroidal component is

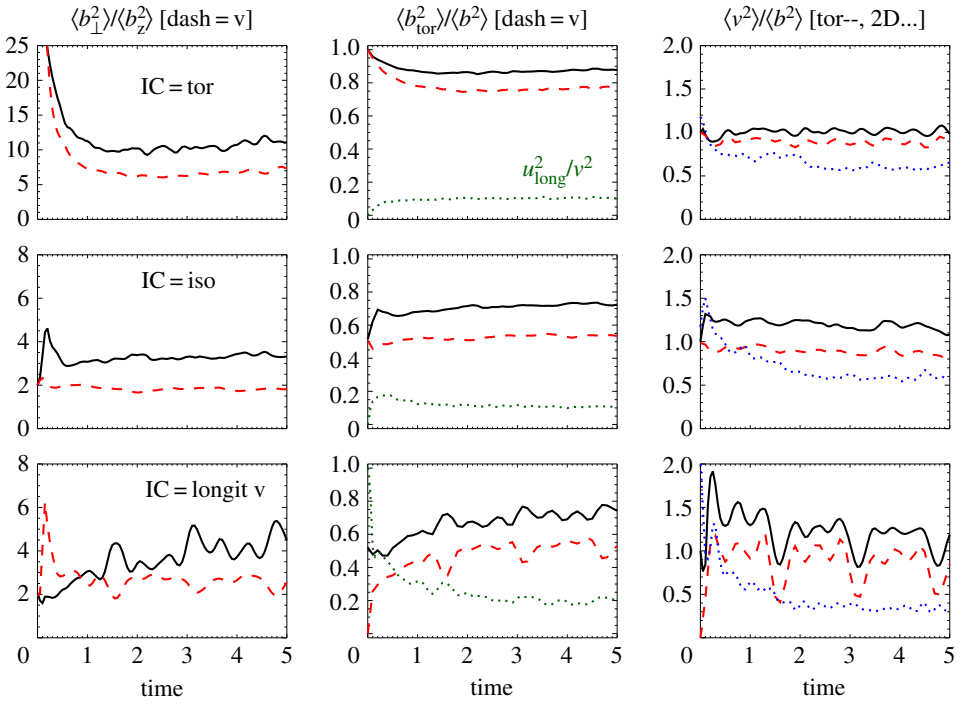

Figure 4. Variance anisotropy quantities from compressible three-dimensional MHD simulations. Each row is for a $\beta_p = 1$ run with a different type of IC. Top: ***b***, ***v*** strictly toroidal. Middle: isotropic, meaning ***b***, ***v*** have equal power in the toroidal and poloidal components. Bottom: ***b*** isotropic, ***v*** purely longitudinal. (Online version in colour.)

less dominant because an $O(M_s^2)$ longitudinal velocity component emerges [120]. The final column of figure 4 displays three different v^2/b^2 ratios: that for all the fluctuations (r_A), that for just the toroidal components (r_A^{tor}), and that for just the $k_\parallel = 0$ components (r_A^{2D}). Although there can be significant fluctuations about the average values, in all cases (i) $r_A^{tor} \approx 1$, which is not inconsistent with this component being strongly Alfvén wave-like, (ii) $r_A^{2D} < 1$ (except at short time), which, as expected, is inconsistent with wave-like features [90], and (iii) $r_A > r_A^{tor}$ is a little bigger than 1.

The energetic dominance of the toroidal fluctuations in these turbulence simulations is consistent with the Wicks *et al.* [118] results; however, solar wind observations also usually report $r_A < 1$, corresponding to 'excess' magnetic energy rather than the 'excess' velocity energy seen here. Part of the explanation may be that the simulations have a two-dimensional energy fraction of $\approx 10\%$ of the fluctuation energy—which is quite different from the typical $\sim 80\%$ two-dimensional–20% slab results discussed in §3. A fuller study exploring a range of β_p values and two-dimensional energy fractions is underway.

5. Summary

Regarding the velocity and magnetic field fluctuations, one can state with confidence that in the solar wind inertial range, observations indicate that they are predominantly polarized transverse to the mean magnetic field, and that their spectral energy distribution is not isotropic. Indeed, there is multi-pronged evidence for fluctuations with quasi-perpendicular wavevectors being considerably more energetic than those with quasi-parallel wavevectors (of comparable magnitude). These features are consistent with channelling of energy towards small perpendicular scales. It appears to be more difficult to move inertial range energy towards small

parallel scales. Thus, dissipation and heating processes that favour large quasi-perpendicular wavenumbers may be of most relevance.

More recently, results extending well into the solar wind dissipation range have been presented and some of these indicate that the spectral and variance anisotropies of the fluctuations may differ from those typically seen in the inertial range. However, for spectral anisotropy the results are not all in accord so that its nature is still uncertain. For example, fits of the slab + 2D kind suggest quasi-parallel wavevectors are energetically important, whereas other techniques often report energetic dominance for quasi-$k_\perp$ fluctuations. For variance anisotropy, observational analyses are more consistent and there are good indications that it progressively weakens with scale, towards isotropy at about the electron gyroradius. Note that at kinetic and smaller length scales the fluctuations can still have nonlinear time scales comparable to the typical wave-based time scales, often $\sim 1/\Omega_{\rm ci}$ [121]. Naturally, additional physics comes into play at kinetic scales. Wave–particle effects, distinct cascades and modified and/or new wave modes may all be significant.

At present, wave-based explanations and turbulence-based explanations are both viable candidates for the observed anisotropies and it may well be that this represents the true situation. New observational data—from upcoming missions such as Solar Orbiter and Solar Probe Plus—should assist with uncovering the specifics of anisotropies at small scales in the solar wind, and thereby further our understanding of heating and dissipation in the medium.

Acknowledgements. We thank K. Kiyani, J.J. Podesta and F. Sahraoui for kindly supplying figures from their papers for reproduction here.

Funding statement. This research was supported in part by the UK STFC, US NSF Solar Terrestrial grant nos. AGS-1063439 and SHINE AGS-1156094, the NASA Heliospheric Grand Challenge project NNX14AI63G and Solar probe Plus ISIS project (SWRI subcontract D99031L), and the NASA/EPSCoR Programme (NNX13AB30A).

Appendix A. Types of spectra and spectral ranges

Turbulence theories and phenomenologies make considerable use of wavevector ($\boldsymbol{k}$) spectra [13,18]. The most fundamental of these is the *modal* spectrum $E(\boldsymbol{k})$, which describes the distribution of energy in three-dimensional wavevector space. The total energy is $E^{\rm tot} = \iiint E(\boldsymbol{k}) {\rm d}^3\boldsymbol{k}$. Several different integrals of the modal spectrum are useful. The *omnidirectional* spectrum is obtained by employing spherical polar coordinates in $\boldsymbol{k}$-space and integrating over the two angular coordinates: $\mathcal{E}(k) = \iint {\rm d}\theta\, {\rm d}\phi k^2 \sin\theta E(k,\theta,\phi)$, and is particularly relevant for isotropic distributions. The *reduced* spectrum (relative to the k_3 direction) is $E^{\rm red}(k_3) = \iint {\rm d}k_1\, {\rm d}k_2 E(k_1,k_2,k_3)$, where k_1,k_2,k_3 denotes some choice of Cartesian coordinates. For measurements made in systems with a strong mean flow—like the solar wind—it can be approximated using a timeseries obtained at a *single* point in space, via the Taylor 'frozen flow' assumption [12,122]; see below. Except in special high symmetry cases, it is not possible to obtain $E(\boldsymbol{k})$ from the omnidirectional or reduced forms [18,123]. This is because the reduced spectrum is a *projection* of the modal spectrum, and hence different modal spectra can yield the same reduced spectrum.

Spacecraft speeds are usually much slower than those of the supersonic solar wind. Thus, for time intervals that are not too long, the measurements made are a timeseries at approximately the same point in space. These datasets can be used to calculate temporal correlation functions and *frequency* power spectra, say $P(f)$. Let the mean solar wind speed be $\boldsymbol{U} = U_{\rm sw}\hat{\boldsymbol{R}}$, where $\hat{\boldsymbol{R}}$ is the unit vector for the heliocentric radius coordinate. Under the Taylor frozen-flow assumption [122], namely that $U_{\rm sw}$ greatly exceeds typical wave speeds and fluctuation speeds, the frequency spectrum is equivalent to a reduced wavenumber spectrum: $E^{\rm red}(k_3) = U_{\rm sw}P(f = k_3 U_{\rm sw}/2\pi)$, where $k_3 = \boldsymbol{k}\cdot\hat{\boldsymbol{R}}$ is the component of $\boldsymbol{k}$ parallel to $\boldsymbol{U}$, and the wavevector components transverse to $\boldsymbol{U}$ have been integrated over [123]. This enables some information about the spatial structure of the turbulence to be obtained from measurements at a single position.

Spectral ranges. For large Reynolds-number isotropic hydrodynamic turbulence, there are three scale (or wavenumber) ranges of particular interest. These are related to two characteristic scales

of a steady turbulent flow: the integral scale[6] $L_{\rm cor} = (\pi/2E^{\rm tot}) \int_0^\infty (\mathcal{E}(k)/k)\,{\rm d}k$ and the Kolmogorov dissipation scale $\ell_{\rm diss} = (\nu^3/\epsilon)^{1/4}$, where ν is the kinematic viscosity of the fluid and ϵ the rate of energy injection. At the large scales is the *energy-containing range*, with scales $\ell \sim L_{\rm cor}$, often associated with the scale of the driving. The *dissipation range* comprises the small scales $\ell \lesssim \ell_{\rm diss}$, and viscous dissipation is the dominant physics there. In between these—and well separated from both of them—is the *inertial range*, $\ell_{\rm diss} \ll \ell \ll L_{\rm cor}$, for which the direct effects of forcing and dissipation are treated as negligible. The physics of the inertial range is then argued to be self-similar, leading to its famous Kolmogorov spectrum $\mathcal{E}(k) = C\epsilon^{2/3}k^{-5/3}$, with C the order unity Kolmogorov constant. MHD turbulence is more complicated, in part because of anisotropies and wave effects associated with mean fields [14]. Plasmas, too, have additional richness.

A few words are in order regarding the definition of the inertial range and, particularly, the dissipation range in solar wind data, because plasma effects lead to some differences from the hydrodynamic case. For common 1 AU (ecliptic) conditions the inertial range frequencies are an MHD-scale band from $\sim 10^{-4}$ to $\sim 10^{-1}$ Hz, and approximate powerlaw behaviour is often seen. The high-frequency end is roughly the proton gyrofrequency, $f_{\rm ci}$, and there is usually a fairly sharp transition about there to a steeper powerlaw, with a slope that shows considerable variation [45].[7] If the solar wind were a viscoresistive magnetofluid, this $f > f_{\rm ci}$ range would correspond to a fluid dissipation range with approximately exponential falloff and dynamics dominated by viscous and resistive diffusion. Instead, however, the solar wind is a strongly ionized plasma and this range may involve dissipation processes that are more complicated than viscous diffusion. For example, dissipation might occur via wave–particle interactions, wave damping and/or further cascades [7–11]. These processes are expected to become relevant at scales near (and smaller than) the proton gyroradius ($\rho_{\rm i}$) and/or proton inertial length ($d_{\rm i} = V_{\rm A}/\Omega_{\rm ci}$). Although the physics is not exclusively dissipative, the solar wind literature still commonly refers to this set of scales as the dissipation range, and we follow this usage herein. An alternative designation is the *dispersion range* [64,124].

Note that when the wavevector energy spectrum is anisotropic, owing to a mean field $\boldsymbol{B}_0$, say, the frequency at which $P(f)$ transitions from the inertial range to the dissipation range can depend on the angle the measurement direction makes with $\boldsymbol{B}_0$ [43,125].

Appendix B. Mean magnetic fields: global and local

An important issue for many types of anisotropy is the scale over which the mean magnetic field is defined. For a *local mean field*, $\boldsymbol{B}_0^{\rm loc}$, it might be the same scale as that of the considered fluctuations, or perhaps 2, 5 or 10 times that. Studies employing either wavelets or structure functions now commonly take this approach. For a global mean field, $\boldsymbol{B}_0$, the averaging occurs over the whole data interval (or simulation domain), so that $\boldsymbol{B}_0$ is uniform. The particular mean field used can lead to significant differences in results [23,100,101]. Possibly the most well-known solar wind case concerns the energy spectrum and how the inertial range slope depends on the angle between the measurement direction and the direction of $\boldsymbol{B}_0$ or $\boldsymbol{B}_0^{\rm loc}$. No systematic difference in slopes is seen when a global field is used, but steeper spectral slopes are seen at small angles when local mean fields are employed (see [6] for a review).

Note that wavelet 'spectra' computed relative to local mean fields are, in fact, not spectra in the classical second-order moment sense [23]. Rather, because the direction of $\boldsymbol{B}_0^{\rm loc}$ is itself a random variable, wavelet 'spectra' also involve third- and higher-order correlations.

Recall that the properties of linear wave modes are typically derived assuming a homogeneous background with a mean magnetic field that is uniform and constant [126]. If one wishes to investigate the properties of wave modes relative to a $\boldsymbol{B}_0^{\rm loc}$, this is clearly a more complicated situation. In the extreme cases where $\boldsymbol{B}_0^{\rm loc}$ is defined over the same scale as the fluctuations,

[6]This is closely related to the correlation scale and the energy-containing scale [13,18].

[7]When the electron gyrofrequency is reached the behaviour changes again, with claims for powerlaws, exponential dependence and combinations of these. See [4] and references therein.

it is possible or even probable that $\boldsymbol{B}_0^{\mathrm{loc}}$ changes *direction* on the same time scale that the fluctuations evolve. It is then difficult to see how features requiring some stableness relative to the $\boldsymbol{B}_0^{\mathrm{loc}}$ direction—for example, $\boldsymbol{k}$ *exactly* perpendicular to $\boldsymbol{B}_0^{\mathrm{loc}}$ for supposed analogues of ion Bernstein modes—can persist long enough to justify their interpretation. Similar comments apply to exactly two-dimensional turbulence. However, because two-dimensional turbulence does not rely on a dispersion relation or specific modal eigenstructures, the exactness of the two-dimensionality is not as relevant, and quasi-two-dimensional turbulence (i.e. allowing large-scale, but not small-scale, dependence on the parallel coordinate) remains a sound concept.

There are other issues associated with averaging intervals that are shorter than a correlation time or correlation length. In particular, such short averaging intervals may produce unconverged spectral estimates, containing stochastic anisotropies owing to undersampling of the data. Separating such distortions from the true signal is difficult. Thus, observations of variance anisotropy do not necessarily imply actual anisotropy of the energy spectrum! See the discussion around equation (2.3) [18–21].

References

1. Richardson JD, Smith CW. 2003 The radial temperature profile of the solar wind. *Geophys. Res. Lett.* **30**, 1206. (doi:10.1029/2002GL016551)
2. Bruno R, Carbone V. 2005 The solar wind as a turbulence laboratory. *Living Rev. Solar Phys.* **2**, 4. (doi:10.12942/lrsp-2005-4)
3. Oughton S, Matthaeus WH. 2005 Parallel and perpendicular cascades in solar wind turbulence. *Nonlinear Process. Geophys.* **12**, 299–310. (doi:10.5194/npg-12-299-2005)
4. Alexandrova O, Chen CHK, Sorriso-Valvo L, Horbury TS, Bale SD. 2013 Solar wind turbulence and the role of ion instabilities. *Space Sci. Rev.* **178**, 101–139. (doi:10.1007/s11214-013-0004-8)
5. Horbury T, Forman MA, Oughton S. 2005 Spacecraft observations of solar wind turbulence: an overview. *Plasma Phys. Controlled Fusion* **47**, B703–B717. (doi:10.1088/0741-3335/47/12B/S52)
6. Horbury TS, Wicks RT, Chen CHK. 2012 Anisotropy in space plasma turbulence: solar wind observations. *Space Sci. Rev.* **172**, 325–342. (doi:10.1007/s11214-011-9821-9)
7. Matthaeus WH, Wan M, Servidio S, Greco A, Osman KT, Oughton S, Dmitruk P. 2015 Intermittency, nonlinear dynamics and dissipation in the solar wind and astrophysical plasmas. *Phil. Trans. R. Soc. A* **373**, 20140154. (doi:10.1098/rsta.2014.0154)
8. Coburn JT, Forman MA, Smith CW, Vasquez BJ, Stawarz JE. 2015 Third-moment descriptions of the interplanetary turbulent cascade, intermittency and back transfer. *Phil. Trans. R. Soc. A* **373**, 20140150. (doi:10.1098/rsta.2014.0150)
9. Gary SP. 2015 Short-wavelength plasma turbulence and temperature anisotropy instabilities: recent computational progress. *Phil. Trans. R. Soc. A* **373**, 20140149. (doi:10.1098/rsta.2014.0149)
10. Goldstein ML, Wicks RT, Perri S, Sahraoui F. 2015 Kinetic scale turbulence and dissipation in the solar wind: key observational results and future outlook. *Phil. Trans. R. Soc. A* **373**, 20140147. (doi:10.1098/rsta.2014.0147)
11. Howes GG. 2015 A dynamical model of plasma turbulence in the solar wind. *Phil. Trans. R. Soc. A* **373**, 20140145. (doi:10.1098/rsta.2014.0145)
12. Frisch U. 1995 *Turbulence*. Cambridge, UK: Cambridge University Press.
13. Pope SB. 2000 *Turbulent flows*. Cambridge, UK: Cambridge University Press.
14. Biskamp D. 2003 *Magnetohydrodynamic turbulence*. Cambridge, UK: Cambridge University Press.
15. Matthaeus WH, Dasso S, Weygand JM, Milano LJ, Smith CW, Kivelson MG. 2005 Spatial correlation of solar-wind turbulence from two-point measurements. *Phys. Rev. Lett.* **95**, 231101. (doi:10.1103/PhysRevLett.95.231101)
16. Weygand JM, Matthaeus WH, Dasso S, Kivelson MG, Kistler LM, Mouikis C. 2009 Anisotropy of the Taylor scale and the correlation scale in plasma sheet and solar wind magnetic field fluctuations. *J. Geophys. Res.* **114**, A07213. (doi:10.1029/2008JA013766)

17. Weygand JM, Matthaeus WH, Dasso S, Kivelson MG. 2011 Correlation and Taylor scale variability in the interplanetary magnetic field fluctuations as a function of solar wind speed. *J. Geophys. Res.* **116**, A08102. (doi:10.1029/2011JA016621)
18. Batchelor GK. 1970 *The theory of homogeneous turbulence*. Cambridge, UK: Cambridge University Press.
19. Bieber JW, Wanner W, Matthaeus WH. 1996 Dominant two-dimensional solar wind turbulence with implications for cosmic ray transport. *J. Geophys. Res.* **101**, 2511–2522. (doi:10.1029/95JA02588)
20. Turner AJ, Gogoberidze G, Chapman SC, Hnat B, Müller WC. 2011 Nonaxisymmetric anisotropy of solar wind turbulence. *Phys. Rev. Lett.* **107**, 095002. (doi:10.1103/PhysRevLett.107.095002)
21. Turner AJ, Gogoberidze G, Chapman SC. 2012 Nonaxisymmetric anisotropy of solar wind turbulence as a direct test for models of magnetohydrodynamic turbulence. *Phys. Rev. Lett.* **108**, 085001. (doi:10.1103/PhysRevLett.108.085001)
22. Matthaeus WH, Goldstein ML. 1982 Stationarity of magnetohydrodynamic fluctuations in the solar wind. *J. Geophys. Res.* **87**, 10 347–10 354. (doi:10.1029/JA087iA12p10347)
23. Matthaeus WH, Servidio S, Dmitruk P, Carbone V, Oughton S, Wan M, Osman KT. 2012 Local anisotropy, higher order statistics, and turbulence spectra. *Astrophys. J.* **750**, 103. (doi:10.1088/0004-637X/750/2/103)
24. Robinson DC, Rusbridge MG. 1971 Structure of turbulence in the zeta plasma. *Phys. Fluids* **14**, 2499–2511. (doi:10.1063/1.1693359)
25. Zweben S, Menyuk C, Taylor R. 1979 Small-scale magnetic fluctuations inside the Macrotor tokamak. *Phys. Rev. Lett.* **42**, 1270–1274. (doi:10.1103/PhysRevLett.42.1270)
26. Montgomery DC, Turner L. 1981 Anisotropic magnetohydrodynamic turbulence in a strong external magnetic field. *Phys. Fluids* **24**, 825–831. (doi:10.1063/1.863455)
27. Montgomery DC. 1982 Major disruption, inverse cascades, and the Strauss equations. *Phys. Scr.* **1982**, 83–88. (doi:10.1088/0031-8949/1982/T2A/009)
28. Shebalin JV, Matthaeus WH, Montgomery D. 1983 Anisotropy in MHD turbulence due to a mean magnetic field. *J. Plasma Phys.* **29**, 525–547. (doi:10.1017/S0022377800000933)
29. Goldreich P, Sridhar S. 1995 Toward a theory of interstellar turbulence: II. Strong Alfvénic turbulence. *Astrophys. J.* **438**, 763–775. (doi:10.1086/175121)
30. Goldreich P, Sridhar S. 1997 Magnetohydrodynamic turbulence revisited. *Astrophys. J.* **485**, 680–688. (doi:10.1086/304442)
31. Oughton S, Wan M, Servidio S, Matthaeus WH. 2013 On the origin of anisotropy in magnetohydrodynamic turbulence: the role of higher-order correlations. *Astrophys. J.* **768**, 10. (doi:10.1088/0004-637X/768/1/10)
32. Crooker NU, Siscoe GL, Russell CT, Smith EJ. 1982 Factors controlling degree of correlation between ISEE 1 and ISEE 3 interplanetary magnetic field measurements. *J. Geophys. Res.* **87**, 2224–2230. (doi:10.1029/JA087iA04p02224)
33. Matthaeus WH, Goldstein ML, Roberts DA. 1990 Evidence for the presence of quasi-two-dimensional nearly incompressible fluctuations in the solar wind. *J. Geophys. Res.* **95**, 20 673–20 683. (doi:10.1029/JA095iA12p20673)
34. Boldyrev S. 2005 On the spectrum of magnetohydrodynamic turbulence. *Astrophys. J.* **626**, L37–L40. (doi:10.1086/431649)
35. Boldyrev S. 2006 Spectrum of magnetohydrodynamic turbulence. *Phys. Rev. Lett.* **96**, 115002. (doi:10.1103/PhysRevLett.96.115002)
36. Cho J, Lazarian A, Vishniac ET. 2002 Simulations of magnetohydrodynamic turbulence in a strongly magnetized region. *Astrophys. J.* **564**, 291–301. (doi:10.1086/324186)
37. Nazarenko SV, Schekochihin AA. 2011 Critical balance in magnetohydrodynamic, rotating and stratified turbulence: towards a universal scaling conjecture. *J. Fluid Mech.* **677**, 134–153. (doi:10.1017/S002211201100067X)
38. Jokipii JR. 1966 Cosmic-ray propagation. I. Charged particles in a random magnetic field. *Astrophys. J.* **146**, 480–487. (doi:10.1086/148912)
39. Chandran BDG. 2000 Scattering of energetic particles by anisotropic magnetohydrodynamic turbulence with a Goldreich–Sridhar power spectrum. *Phys. Rev. Lett.* **85**, 4656–4659. (doi:10.1103/PhysRevLett.85.4656)
40. Dmitruk P, Matthaeus WH. 2009 Waves and turbulence in magnetohydrodynamic direct numerical simulations. *Phys. Plasmas* **16**, 062304. (doi:10.1063/1.3148335)

41. Parashar TN, Servidio S, Shay MA, Breech B, Matthaeus WH. 2011 Effect of driving frequency on excitation of turbulence in a kinetic plasma. *Phys. Plasmas* **18**, 092302. (doi:10.1063/1.3630926)
42. Klein KG, Howes GG, TenBarge JM, Bale SD, Chen CHK, Salem CS. 2012 Using synthetic spacecraft data to interpret compressible fluctuations in solar wind turbulence. *Astrophys. J.* **755**, 159. (doi:10.1088/0004-637X/755/2/159)
43. Leamon RJ, Smith CW, Ness NF, Matthaeus WH, Wong HK. 1998 Observational constraints on the dynamics of the interplanetary magnetic field dissipation range. *J. Geophys. Res.* **103**, 4775–4787. (doi:10.1029/97JA03394)
44. Smith CW. 2003 The geometry of turbulent magnetic fluctuations at high heliographic latitude. In *Solar Wind Ten: Proc. 10th Int. Solar Wind Conf.*, vol. 679 (eds M Velli, R Bruno, F Malara), pp. 413–416. Melville, NY: AIP.
45. Hamilton K, Smith CW, Vasquez BJ, Leamon RJ. 2008 Anisotropies and helicities in the solar wind inertial and dissipation ranges at 1 AU. *J. Geophys. Res.* **113**, A01106. (doi:10.1029/2007JA012559)
46. MacBride BT, Smith CW, Vasquez BJ. 2010 Inertial-range anisotropies in the solar wind from 0.3 to 1 AU: Helios 1 observations. *J. Geophys. Res.* **115**, A07105. (doi:10.1029/2009JA014939)
47. Smith CW, Vasquez BJ, Hollweg JV. 2012 Observational constraints on the role of cyclotron damping and kinetic Alfvén waves in the solar wind. *Astrophys. J.* **745**, 8. (doi:10.1088/0004-637X/745/1/8)
48. Horbury TS, Forman M, Oughton S. 2008 Anisotropic scaling of magnetohydrodynamic turbulence. *Phys. Rev. Lett.* **101**, 175005. (doi:10.1103/PhysRevLett.101.175005)
49. Osman KT, Horbury TS. 2009 Multi-spacecraft measurement of anisotropic power levels and scaling in solar wind turbulence. *Ann. Geophys.* **27**, 3019–3025. (doi:10.5194/angeo-27-3019-2009)
50. Osman KT, Horbury TS. 2009 Quantitative estimates of the slab and 2-D power in solar wind turbulence using multispacecraft data. *J. Geophys. Res.* **114**, A06103. (doi:10.1029/2008JA014036)
51. Tessein JA, Smith CW, Vasquez BJ, Skoug RM. 2011 Turbulence associated with corotating interaction regions at 1 AU: inertial and dissipation range magnetic field spectra. *J. Geophys. Res.* **116**, A10104. (doi:10.1029/2011JA016647)
52. Dasso S, Milano LJ, Matthaeus WH, Smith CW. 2005 Anisotropy in fast and slow solar wind fluctuations. *Astrophys. J.* **635**, L181–L184. (doi:10.1086/499559)
53. Wicks RT, Horbury TS, Chen CHK, Schekochihin AA. 2010 Power and spectral index anisotropy of the entire inertial range of turbulence in the fast solar wind. *Mon. Not. R. Astron. Soc.* **407**, L98–L101. (doi:10.1111/j.1745-3933.2010.00898.x)
54. MacBride BT, Smith CW, Forman MA. 2008 The turbulent cascade at 1 AU: energy transfer and the third-order scaling for MHD. *Astrophys. J.* **679**, 1644–1660. (doi:10.1086/529575)
55. Oughton S, Priest ER, Matthaeus WH. 1994 The influence of a mean magnetic field on three-dimensional MHD turbulence. *J. Fluid Mech.* **280**, 95–117. (doi:10.1017/S0022112094002867)
56. Cho J, Vishniac ET. 2000 The anisotropy of magnetohydrodynamic Alfvénic turbulence. *Astrophys. J.* **539**, 273–282. (doi:10.1086/309213)
57. Zhou Y, Matthaeus WH, Dmitruk P. 2004 Magnetohydrodynamic turbulence and timescales in astrophysical and space plasmas. *Rev. Mod. Phys.* **76**, 1015–1035. (doi:10.1103/RevModPhys.76.1015)
58. Zhou Y, Matthaeus WH. 2005 Phenomenology treatment of magnetohydrodynamic turbulence with nonequipartition and anisotropy. *Phys. Plasmas* **12**, 056503. (doi:10.1063/1.1887187)
59. Smith CW, Vasquez BJ, Hamilton K. 2006 Interplanetary magnetic fluctuation anisotropy in the inertial range. *J. Geophys. Res.* **111**, A09111. (doi:10.1029/2006JA011651)
60. Podesta JJ. 2009 Dependence of solar-wind power spectra on the direction of the local mean magnetic field. *Astrophys. J.* **698**, 986–999. (doi:10.1088/0004-637X/698/2/986)
61. Luo QY, Wu DJ. 2010 Observations of anisotropic scaling of solar wind turbulence. *Astrophys. J.* **714**, L138–L141. (doi:10.1088/2041-8205/714/1/L138)
62. Forman MA, Wicks RT, Horbury TS. 2011 Detailed fit of 'critical balance' theory to solar wind turbulence measurements. *Astrophys. J.* **733**, 76. (doi:10.1088/0004-637X/733/2/76)
63. He J, Tu C, Marsch E, Bourouaine S, Pei Z. 2013 Radial evolution of the wavevector anisotropy of solar wind turbulence between 0.3 and 1 AU. *Astrophys. J.* **773**, 72. (doi:10.1088/0004-637X/773/1/72)

64. Gary SP, Smith CW. 2009 Short-wavelength turbulence in the solar wind: linear theory of whistler and kinetic Alfvén fluctuations. *J. Geophys. Res.* **114**, A12105. (doi:10.1029/2009JA014525)
65. Podesta JJ, Gary SP. 2011 Effect of differential flow of alpha particles on proton pressure anisotropy instabilities in the solar wind. *Astrophys. J.* **742**, 41. (doi:10.1088/0004-637X/742/1/41)
66. Klein KG, Howes GG, TenBarge JM, Podesta JJ. 2014 Physical interpretation of the angle-dependent magnetic helicity spectrum in the solar wind: the nature of turbulent fluctuations near the proton gyroradius scale. *Astrophys. J.* **785**, 138. (doi:10.1088/0004-637X/785/2/138)
67. Sahraoui F, Goldstein ML, Belmont G, Canu P, Rezeau L. 2010 Three dimensional anisotropic *k* spectra of turbulence at subproton scales in the solar wind. *Phys. Rev. Lett.* **105**, 131101. (doi:10.1103/PhysRevLett.105.131101)
68. Tjulin A, Pinçon JL, Sahraoui F, André M, Cornilleau-Wehrlin N. 2005 The k-filtering technique applied to wave electric and magnetic field measurements from the Cluster satellites. *J. Geophys. Res.* **110**, A11224. (doi:10.1029/2005JA011125)
69. Sahraoui F, Belmont G, Goldstein ML, Rezeau L. 2010 Limitations of multispacecraft data techniques in measuring wave number spectra of space plasma turbulence. *J. Geophys. Res.* **115**, A04206. (doi:10.1029/2009JA014724)
70. Chen CHK, Horbury TS, Schekochihin AA, Wicks RT, Alexandrova O, Mitchell J. 2010 Anisotropy of solar wind turbulence between ion and electron scales. *Phys. Rev. Lett.* **104**, 255002. (doi:10.1103/PhysRevLett.104.255002)
71. Narita Y, Gary SP, Saito S, Glassmeier KH, Motschmann U. 2011 Dispersion relation analysis of solar wind turbulence. *Geophys. Res. Lett.* **38**, L05101. (doi:10.1029/2010GL046588)
72. Narita Y, Comişel H, Motschmann U. 2014 Spatial structure of ion-scale plasma turbulence. *Front. Phys.* **2**, 13. (doi:10.3389/fphy.2014.00013)
73. Comişel H, Narita Y, Motschmann U. 2014 Wavevector anisotropy of plasma turbulence at ion kinetic scales: solar wind observations and hybrid simulations. *Nonlinear Process. Geophys.* **21**, 1075–1083. (doi:10.5194/npg-21-1075-2014)
74. Roberts OW, Li X, Li B. 2013 Kinetic plasma turbulence in the fast solar wind measured by Cluster. *Astrophys. J.* **769**, 58. (doi:10.1088/0004-637X/769/1/58)
75. Perschke C, Narita Y, Motschmann U, Glassmeier KH. 2014 Multi-spacecraft observations of linear modes and sideband waves in ion-scale solar wind turbulence. *Astrophys. J.* **793**, L25. (doi:10.1088/2041-8205/793/2/L25)
76. Narita Y, Sahraoui F, Goldstein ML, Glassmeier KH. 2010 Magnetic energy distribution in the four-dimensional frequency and wave vector domain in the solar wind. *J. Geophys. Res.* **115**, A04101. (doi:10.1029/2009JA014742)
77. Narita Y, Glassmeier KH, Sahraoui F, Goldstein ML. 2010 Wave-vector dependence of magnetic-turbulence spectra in the solar wind. *Phys. Rev. Lett.* **104**, 171101. (doi:10.1103/PhysRevLett.104.171101)
78. He J, Tu C, Marsch E, Yao S. 2012 Reproduction of the observed two-component magnetic helicity in solar wind turbulence by a superposition of parallel and oblique Alfvén waves. *Astrophys. J.* **749**, 86. (doi:10.1088/0004-637X/749/1/86)
79. Bieber JW, Matthaeus WH, Smith CW, Wanner W, Kallenrode M, Wibberenz G. 1994 Proton and electron mean free paths: the Palmer consensus revisited. *Astrophys. J.* **420**, 294–306. (doi:10.1086/173559)
80. Shalchi A, Bieber JW, Matthaeus WH, Schlickeiser R. 2006 Parallel and perpendicular transport of heliospheric cosmic rays in an improved dynamical turbulence model. *Astrophys. J.* **642**, 230–243. (doi:10.1086/500728)
81. Pei C, Bieber JW, Breech B, Burger RA, Clem J, Matthaeus WH. 2010 Cosmic ray diffusion tensor throughout the heliosphere. *J. Geophys. Res.* **115**, A03103. (doi:10.1029/2009JA014705)
82. Bondeson A. 1985 Cascade properties of shear Alfvén turbulence. *Phys. Fluids* **28**, 2406–2411. (doi:10.1063/1.865246)
83. Grappin R. 1986 Onset and decay of two-dimensional magnetohydrodynamic turbulence with velocity-magnetic field correlation. *Phys. Fluids* **29**, 2433–2443. (doi:10.1063/1.865536)
84. Galtier S, Nazarenko SV, Newell AC, Pouquet A. 2000 A weak turbulence theory for incompressible magnetohydrodynamics. *J. Plasma Phys.* **63**, 447–488. (doi:10.1017/S0022377899008284)

85. Galtier S, Nazarenko SV, Newell AC, Pouquet A. 2002 Anisotropic turbulence of shear-Alfvén waves. *Astrophys. J.* **564**, L49–L52. (doi:10.1086/338791)
86. Gary SP. 2013 Test for wavevector anisotropies in plasma turbulence cascades. *Astrophys. J.* **769**, 36. (doi:10.1088/0004-637X/769/1/36)
87. Carbone V, Veltri P. 1990 A shell model for anisotropic magnetohydrodynamic turbulence. *Geophys. Astrophys. Fluid Dyn.* **52**, 153–181. (doi:10.1080/03091929008219845)
88. Maron J, Goldreich P. 2001 Simulations of incompressible magnetohydrodynamic turbulence. *Astrophys. J.* **554**, 1175–1196. (doi:10.1086/321413)
89. Milano LJ, Matthaeus WH, Dmitruk P, Montgomery DC. 2001 Local anisotropy in incompressible magnetohydrodynamic turbulence. *Phys. Plasmas* **8**, 2673–2681. (doi:10.1063/1.1369658)
90. Bigot B, Galtier S, Politano H. 2008 Development of anisotropy in incompressible magnetohydrodynamic turbulence. *Phys. Rev. E* **78**, 066301. (doi:10.1103/PhysRevE.78.066301)
91. Nazarenko S. 2011 *Wave turbulence*. Lecture Notes in Physics, vol. 825. Berlin, Germany: Springer.
92. Meyrand R, Kiyani KH, Galtier S. 2014 Intermittency in weak magnetohydrodynamic turbulence. (http://arxiv.org/abs/1409.2092)
93. Wan M, Oughton S, Servidio S, Matthaeus WH. 2012 von Kármán self-preservation hypothesis for magnetohydrodynamic turbulence and its consequences for universality. *J. Fluid Mech.* **697**, 296–315. (doi:10.1017/jfm.2012.61)
94. de Kármán T, Howarth L. 1938 On the statistical theory of isotropic turbulence. *Proc. R. Soc. Lond. A* **164**, 192–215. (doi:10.1098/rspa.1938.0013)
95. Chandrasekhar S. 1951 The invariant theory of isotropic turbulence in magneto-hydrodynamics. *Proc. R. Soc. Lond. A* **204**, 435–449. (doi:10.1098/rspa.1951.0001)
96. Chandrasekhar S. 1951 The invariant theory of isotropic turbulence in magneto-hydrodynamics. II. *Proc. R. Soc. Lond. A* **207**, 301–306. (doi:10.1098/rspa.1951.0118)
97. Politano H, Pouquet A. 1998 von Kármán–Howarth equation for magnetohydrodynamics and its consequences on third-order longitudinal structure and correlation functions. *Phys. Rev. E* **57**, R21–R24. (doi:10.1103/PhysRevE.57.R21)
98. Chapman SC, Hnat B. 2007 Quantifying scaling in the velocity field of the anisotropic turbulent solar wind. *Geophys. Res. Lett.* **34**, L17103. (doi:10.1029/2007GL030518)
99. Perri S, Yordanova E, Carbone V, Veltri P, Sorriso-Valvo L, Bruno R, André M. 2009 Magnetic turbulence in space plasmas: scale-dependent effects of anisotropy. *J. Geophys. Res.* **114**, A02102. (doi:10.1029/2008JA013491)
100. Chen CHK, Mallet A, Yousef TA, Schekochihin AA, Horbury TS. 2011 Anisotropy of Alfvénic turbulence in the solar wind and numerical simulations. *Mon. Not. R. Astron. Soc.* **415**, 3219–3226. (doi:10.1111/j.1365-2966.2011.18933.x)
101. TenBarge JM, Podesta JJ, Klein KG, Howes GG. 2012 Interpreting magnetic variance anisotropy measurements in the solar wind. *Astrophys. J.* **753**, 107. (doi:10.1088/0004-637X/753/2/107)
102. Kiyani KH, Chapman SC, Sahraoui F, Hnat B, Fauvarque O, Khotyaintsev YV. 2013 Enhanced magnetic compressibility and isotropic scale invariance at sub-ion Larmor scales in solar wind turbulence. *Astrophys. J.* **763**, 10. (doi:10.1088/0004-637X/763/1/10)
103. Belcher JW, Davis Jr L. 1971 Large-amplitude Alfvén waves in the interplanetary medium, 2. *J. Geophys. Res.* **76**, 3534–3563. (doi:10.1029/JA076i016p03534)
104. Bavassano B, Dobrowolny M, Mariani F, Ness NF. 1982 Radial evolution of power spectra of interplanetary Alfvénic turbulence. *J. Geophys. Res.* **87**, 3617–3622. (doi:10.1029/JA087iA05p03617)
105. Bruno R, Bavassano B, Pietropaolo E, Carbone V, Veltri P. 1999 Effects of intermittency on interplanetary velocity and magnetic field fluctuations anisotropy. *Geophys. Res. Lett.* **26**, 3185–3188. (doi:10.1029/1999GL010668)
106. Klein LW, Roberts DA, Goldstein ML. 1991 Anisotropy and minimum variance directions of solar wind fluctuations in the outer heliosphere. *J. Geophys. Res.* **96**, 3779–3788. (doi:10.1029/90JA02240)
107. Horbury T, Balogh A, Forsyth RJ, Smith EJ. 1995 Anisotropy of inertial range turbulence in the polar heliosphere. *Geophys. Res. Lett.* **22**, 3405–3408. (doi:10.1029/95GL03012)

108. Salem CS, Howes GG, Sundkvist D, Bale SD, Chaston CC, Chen CHK, Mozer FS. 2012 Identification of kinetic Alfvén wave turbulence in the solar wind. *Astrophys. J.* **745**, L9. (doi:10.1088/2041-8205/745/1/L9)
109. Podesta JJ, TenBarge JM. 2012 Scale dependence of the variance anisotropy near the proton gyroradius scale: additional evidence for kinetic Alfvén waves in the solar wind at 1 AU. *J. Geophys. Res.* **117**, A10106. (doi:10.1029/2012JA017724)
110. Alexandrova O, Carbone V, Veltri P, Sorriso-Valvo L. 2008 Small-scale energy cascade of the solar wind turbulence. *Astrophys. J.* **674**, 1153–1157. (doi:10.1086/524056)
111. Podesta JJ. 2013 Evidence of kinetic Alfvén waves in the solar wind at 1 AU. *Solar Phys.* **286**, 529–548. (doi:10.1007/s11207-013-0258-z)
112. Sonnerup BUÖ, Cahill LJ. 1967 Magnetopause structure and attitude from Explorer 12 observations. *J. Geophys. Res.* **72**, 171–183. (doi:10.1029/JZ072i001p00171)
113. Saito S, Gary SP, Li H, Narita Y. 2008 Whistler turbulence: particle-in-cell simulations. *Phys. Plasmas* **15**, 102305. (doi:10.1063/1.2997339)
114. Chen CHK, Boldyrev S, Xia Q, Perez JC. 2013 Nature of subproton scale turbulence in the solar wind. *Phys. Rev. Lett.* **110**, 225002. (doi:10.1103/PhysRevLett.110.225002)
115. Dmitruk P, Matthaeus WH. 2003 Low-frequency waves and turbulence in an open magnetic region: timescales and heating efficiency. *Astrophys. J.* **597**, 1097–1105. (doi:10.1086/378636)
116. Ghosh S, Thomson DJ, Matthaeus WH, Lanzerotti LJ. 2009 Coexistence of turbulence and discrete modes in the solar wind. *J. Geophys. Res.* **114**, A08106. (doi:10.1029/2009JA014092)
117. Parashar TN, Servidio S, Breech B, Shay MA, Matthaeus WH. 2010 Kinetic driven turbulence: structure in space and time. *Phys. Plasmas* **17**, 102304. (doi:10.1063/1.3486537)
118. Wicks RT, Forman MA, Horbury TS, Oughton S. 2012 Power anisotropy in the magnetic field power spectral tensor of solar wind turbulence. *Astrophys. J.* **746**, 103. (doi:10.1088/0004-637X/746/1/103)
119. Matthaeus WH, Ghosh S, Oughton S, Roberts DA. 1996 Anisotropic three-dimensional MHD turbulence. *J. Geophys. Res.* **101**, 7619–7629. (doi:10.1029/95JA03830)
120. Zank GP, Matthaeus WH. 1993 Nearly incompressible fluids. II: Magnetohydrodynamics, turbulence, and waves. *Phys. Fluids A* **5**, 257–273. (doi:10.1063/1.858780)
121. Matthaeus WH *et al.* 2014 Nonlinear and linear timescales near kinetic scales in solar wind turbulence. *Astrophys. J.* **790**, 155. (doi:10.1088/0004-637X/790/2/155)
122. Taylor GI. 1938 The spectrum of turbulence. *Proc. R. Soc. Lond. A* **164**, 476–490. (doi:10.1098/rspa.1938.0032)
123. Fredricks RW, Coroniti FV. 1976 Ambiguities in the deduction of rest frame fluctuation spectrums from spectrums computed in moving frames. *J. Geophys. Res.* **81**, 5591–5595. (doi:10.1029/JA081i031p05591)
124. Stawicki O, Gary SP, Li H. 2001 Solar wind magnetic fluctuation spectra: dispersion versus damping. *J. Geophys. Res.* **106**, 8273–8281. (doi:10.1029/2000JA000446)
125. Chen CHK, Wicks RT, Horbury TS, Schekochihin AA. 2010 Interpreting power anisotropy measurements in plasma turbulence. *Astrophys. J.* **711**, L79–L83. (doi:10.1088/2041-8205/711/2/L79)
126. Gary SP. 1993 *Theory of space plasma microinstabilities*. New York, NY: Cambridge University Press.